

Hysteresis and phase transitions in a lattice regularization of an ill-posed forward-backward diffusion equation

Michael Helmers*

Michael Herrmann†

March 3, 2022

Abstract

We consider a lattice regularization for an ill-posed diffusion equation with trilinear constitutive law and study the dynamics of phase interfaces in the parabolic scaling limit. Our main result guarantees for a certain class of single-interface initial data that the lattice solutions satisfy asymptotically a free boundary problem with hysteretic Stefan condition. The key challenge in the proof is to control the microscopic fluctuations that are inevitably produced by the backward diffusion when a particle passes the spinodal region.

Keywords: *multi-scale analysis for gradient flows, regularization of ill-posed diffusion equations hysteresis and phase transitions, interface propagation in discrete media*

MSC (2010): 34A33, 35R25, 37L60, 74N20, 74N30

Contents

1	Introduction	1
1.1	Overview of the key effects	4
1.2	Multiple scales and fluctuations	6
1.3	Main result and plan of paper	9
1.4	On the numerical simulations	10
2	Properties of the lattice dynamics	11
2.1	Existence of single-interface solutions	11
2.2	Lower bound for the waiting time	14
2.3	Family of entropy inequalities	16
3	Analysis of the spinodal fluctuations	17
3.1	Prototypical spinodal problem	18
3.2	Spinodal fluctuations	20
3.3	Local fluctuation estimates	21
3.4	Global fluctuation estimates	23
3.5	Regularity of fluctuations	26
4	Justification of the hysteretic free boundary problem	29
4.1	Compactness results	29
4.2	Passage to the macroscopic limit	32

1 Introduction

Forward-backward diffusion problems arise in many branches of physics and materials science [Ell85, BBPU93], mathematical biology [Pad04, HPO04], and technology [PM90] and lead to complex and intriguing mathematical problems. The simplest dynamical model for a one-dimensional continuous medium would be the nonlinear parabolic PDE

$$\partial_\tau U = \partial_\xi^2 P, \quad P := \Phi'(U) \quad (1.1)$$

*Rheinische Friedrichs-Wilhelm-Universität Bonn, helmers@iam.uni-bonn.de.

†Westfälische Wilhelms-Universität Münster, michael.herrmann@uni-muenster.de.

with time $\tau \geq 0$, space $\xi \in \mathbb{R}$, and non-monotone Φ' , but the corresponding Cauchy problem is ill-posed. To overcome this difficulty, a well-known approach is to consider microscopic regularizations with length parameter $0 < \varepsilon \ll 1$ that take into account small-scale effects and complement (1.1) by additional terms and dynamical laws. The latter depend on the particular choice of Φ' and in what follows we focus on a typical setting in materials science, where Φ' is the bistable derivative of a double-well potential Φ . We also assume that Φ' and Φ are odd and even, respectively, and mention that a bistable function is sometimes called cubic-type as its graph consists of two increasing branches which are separated by an decreasing one.

In the literature, a lot of attention has been paid to the Cahn-Hilliard equation

$$\partial_\tau U = \partial_\xi^2 P - \varepsilon^2 \partial_\xi^4 U \quad (1.2)$$

and the so-called viscous approximation

$$\partial_\tau U = \partial_\xi^2 P + \varepsilon^2 \partial_\tau \partial_\xi^2 U, \quad (1.3)$$

but in this paper we study the spatially discrete regularization

$$\dot{u}_j(t) = \Delta p_j(t), \quad p_j = \Phi'(u_j(t)) \quad (1.4)$$

with microscopic time $t \geq 0$, particle index $j \in \mathbb{Z}$, and standard Laplacian Δ on \mathbb{Z} , that is

$$\Delta v_j = v_{j+1} + v_{j-1} - 2v_j. \quad (1.5)$$

This lattice ODE is linked to the PDE (1.1) by the parabolic scaling

$$\tau := \varepsilon^2 t, \quad \xi := \varepsilon j \quad (1.6)$$

and the formal identification

$$u_j(t) \cong U(\varepsilon^2 t, \varepsilon j), \quad p_j(t) \cong P(\varepsilon^2 t, \varepsilon j), \quad (1.7)$$

whereby we can regard (1.4) as a spatial semi-discretization of (1.1) or, conversely, the PDE (1.1) as the naive continuum limit of the lattice (1.4).

Of particular interest in the analysis of any regularization is the sharp-interface limit $\varepsilon \rightarrow 0$ since it gives rise to phase interfaces, that is, curves $\xi = \Xi(\tau)$ which separate space-time regions in which U is confined to either one of the convex components of Φ (usually called *phases*). The dynamics of such interface curves have to be determined by a free boundary problem that couples the – now locally well-posed – bulk diffusion (1.1) for U on either side of the interface with certain conditions for Ξ . The *Stefan condition*

$$\frac{d\Xi}{d\tau} \llbracket U \rrbracket + \llbracket \partial_\xi P \rrbracket = 0, \quad \llbracket P \rrbracket = 0, \quad (1.8)$$

where $\llbracket \cdot \rrbracket$ denotes the jump across the interface, guarantees for all models that (1.1) holds in a distributional sense across the interface but the evolution of (U, Ξ) depends on another interface condition which encodes the details of the microscopic regularization. For the Cahn-Hilliard equation (1.2), the additional law reads

$$P = 0 \quad (1.9)$$

and fixes the value of P according to Maxwell's local equilibrium criterion. The validity of the free boundary problem (1.1), (1.8) and (1.9) has been proven rigorously in [BBMN12].

Heuristic arguments indicate that the sharp-interface limit of the viscous approximation is more involved since the interface value of P is no longer known as $\varepsilon \rightarrow 0$ but depends in a hysteretic manner on both the state of the system and the propagation direction of the interface. More precisely,

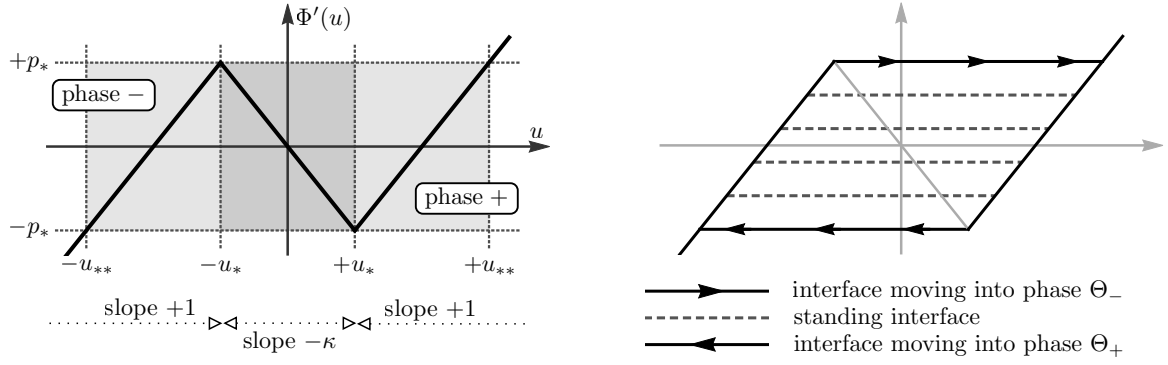


Figure 1.1: *Left Panel.* Graph of the piecewise linear function Φ' as defined in (1.13). The gray boxes represent the intervals I_* and I_{**} from (1.15) and the corresponding double well potential is given in (1.17). *Right panel.* Cartoons of the hysteresis loop for macroscopic phase interfaces. Notice that the interface moves from the phase Θ_+ into the phase Θ_- if and only if the particles at the interface transit the other way round from Θ_- to Θ_+ and that $\llbracket P \rrbracket = 0$ implies $\llbracket U \rrbracket = \pm 2$.

numerical experiments and formal asymptotic analysis as carried out in [Plo94, EP04] predict that the viscous approximation supports both standing and moving interfaces according to the flow rule

$$P = -p_* \text{ for } \frac{d\Xi}{d\tau} \llbracket U \rrbracket > 0, \quad P = +p_* \text{ for } \frac{d\Xi}{d\tau} \llbracket U \rrbracket < 0, \quad \frac{d\Xi}{d\tau} = 0 \text{ for } P \in [-p_*, +p_*], \quad (1.10)$$

where $\pm p_*$ are the two local extrema of the odd function Φ' . The key argument in this derivation is that any reasonable limit for $\varepsilon \rightarrow 0$ satisfies the entropy inequality

$$\partial_\tau \eta(U) - \partial_\xi (\mu(P) \partial_\xi P) \leq 0, \quad (1.11)$$

where the entropy flux η and the entropy density μ can be chosen arbitrarily as long as they comply with

$$\eta' = \mu \circ \Phi', \quad \mu' \geq 0. \quad (1.12)$$

The main tasks for a rigorous justification of the hysteretic flow rule (1.10) or, equivalently, of (1.11) is to show the existence of a smooth interface curve Ξ and to derive ε -uniform a priori estimates that guarantee the strong convergence of the fields as well as the regularity of the limit P . Although there is an extensive literature on the viscous approximation, see the discussion below, we are not aware of any rigorous result that links the hysteretic free boundary problem to the sharp interface limit of (1.3).

For the lattice ODE (1.4), which can also be written as $\dot{w}_j = \nabla_- \Phi'(\nabla_+ w_j)$ with $u_j = \nabla_+ w_j = w_{j+1} - w_j$, one can easily adapt the asymptotic arguments from [Plo94, EP04] to show heuristically that the limit dynamics are governed by the same hysteretic free boundary problem as for the viscous approximation. Moreover, this micro-to-macro transition has been made rigorous in two cases: (i) in [GN11, BGN13] for generic bistable Φ' and initial data that give rise to standing interfaces only, and (ii) by the authors in [HH13] for bilinear Φ' and a suitable class of well-prepared initial data. The latter is to our knowledge the only available rigorous microscopic justification for macroscopic phase interfaces that are driven by hysteric jump conditions. We also refer to [ES08, EG09] for coarsening in discrete forward-backward diffusion lattices with monostable Φ' and to [GST13, GT16] for other systems with spatially distributed hysteresis.

In the current paper, we extend the rigorous analysis from [HH13] to the case of trilinear Φ' . At first glance, the step from bilinear to trilinear seems to be a minor improvement only but the mathematical analysis of the trilinear case is significantly more involved because the spinodal region is no longer degenerate. In particular, microscopic phase transitions are no longer instantaneous processes related to temporal jumps but take a certain time as the particles have to move through the spinodal region. The novel challenge is that the backward diffusion during each spinodal visit produces strong microscopic fluctuations which have to be controlled on the macroscopic scale. The

main achievement of the present paper consists, roughly speaking, in the derivation of asymptotic formulas and estimates for the creation and subsequent amplitude decay of the fluctuations which finally ensure that the lattice data converge as $\varepsilon \rightarrow 0$ to regular macroscopic fields. Moreover, some of the arguments derived below can be generalized to genuinely nonlinear bistable functions Φ' .

In what follows we always suppose – see Figure 1.1 for an illustration – that the lattice ODE (1.4) is complemented by

$$\Phi'(u) := \begin{cases} u + 1 & \text{if } u \leq -u_*, \\ u - 1 & \text{if } u \geq +u_*, \\ -\kappa u & \text{if } -u_* < u < +u_*, \end{cases} \quad (1.13)$$

where $\kappa \in (0, \infty)$ is a free slope-parameter and

$$\pm p_* = \Phi'(\mp u_*) = \Phi'(\pm u_{**}), \quad u_* := \frac{1}{1 + \kappa}, \quad p_* := \frac{\kappa}{1 + \kappa}, \quad u_{**} := \frac{1 + 2\kappa}{1 + \kappa} \quad (1.14)$$

In particular, the bilinear case $\Phi'(u) = u - \text{sgn}(u)$ corresponds to $\kappa = \infty$ while for $\kappa \rightarrow 0$ there is no backward diffusion anymore and the PDE (1.1) becomes degenerate-parabolic.

Before we discuss the dynamical properties of the lattice ODE (1.4), we give a brief and non-exhaustive overview of the literature concerning the viscous approximation (1.3), which can also be formulated as $\partial_\tau W = \partial_\xi \Phi'(\partial_\xi W) + \varepsilon \partial_\tau \partial_\xi^2 W$, where $U = \partial_\xi W$. Moreover, some authors refer to interfaces as phase boundaries, and a standing interface is often called steady.

The initial value problem for (1.3) has been studied in [Pad04, NCP91], and [BCT17] provides existence and uniqueness results for a broader class of regularizing PDEs. Numerical schemes are proposed and analyzed in [EP04, Pie10, LM12] – see also the discussion at the end of §1 – and [NCP91] investigates the multitude of steady states and their dynamical stability with respect to (1.3). Moreover, [Plo94, EP04] characterize the limit $\varepsilon \rightarrow 0$ in the framework of Young measures and entropy inequalities but we already mentioned that the rigorous justification of the limit model has not yet been achieved.

The existence and uniqueness of two-phase entropy solutions to the limiting problem (1.1), (1.8), and (1.11) have been proven in [MTT09] for a trilinear nonlinearity as in (1.13), and [Vis06] studies the existence and uniqueness problem for an equivalent formulation in terms of a parabolic PDE that comprises a spatial family of temporal hysteresis operators. [GT10, LM12] discuss the special case of Riemann initial data and provide explicit formulas for the corresponding self-similar solutions with moving or standing interface. Notice also that the ill-posed forward-backward equation (1.1) admits in general – i.e., without entropy conditions and two-phase assumption – a plethora of solutions, see [Höl83, Zha06] as well as [Ter14, Ter15] for recent results and a discussion of the literature concerning solutions that penetrate the spinodal region. Measure-valued solutions to (1.1) have also been studied, see [Plo94, YW03, EP04, ST10, ST11, BST16] and the references therein.

1.1 Overview of the key effects

The nonlinear lattice (1.4), (1.13) exhibits a complex dynamical behavior since the non-monotonicity of Φ' implies that each particle u_j can either diffuse forwards with regular coefficient $\Phi''(u_j(t)) > 0$ or backwards with $\Phi''(u_j(t)) < 0$. In order to illustrate the different phenomena we next discuss some numerical simulations of finite lattices $j = 1, \dots, N$ with natural scaling parameter $\varepsilon := 1/N$ and homogeneous Neumann conditions, see §1.4 for more details. In particular, we regard the lattice data for large N as discrete sampling of macroscopic fields by scaling time and space but not amplitude according to (1.7), and rely on the following conventions and abbreviations for the interpretation of the numerical results.

Notation 1.1 (Phases and intervals). We refer to the different connected components of the set $\{u : \Phi''(u) > 0\}$ as *phases* and write

$$\Theta_- := (-\infty, -u_*) \quad \text{for the --phase,} \quad \Theta_+ := (+u_*, \infty) \quad \text{for the +-phase,}$$

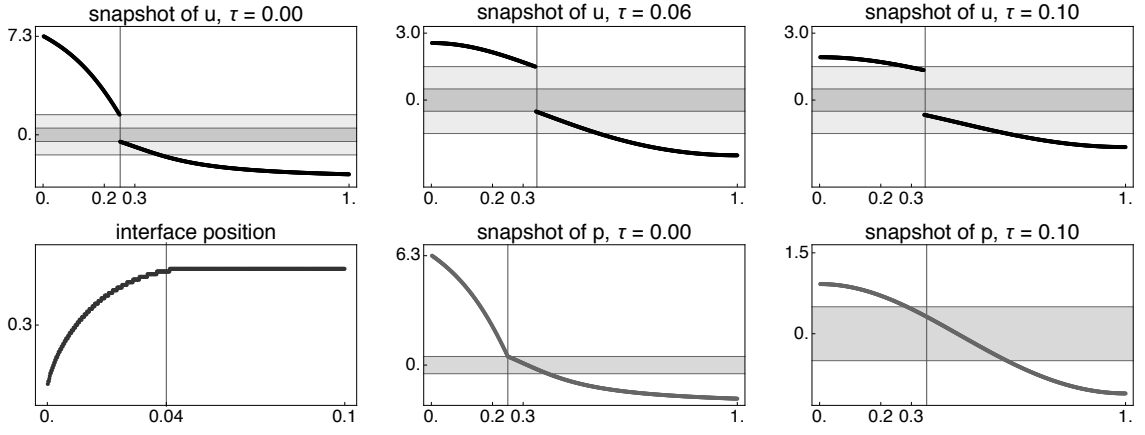


Figure 1.2: Numerical example with single-interface data, computed with Neumann boundary conditions and $\kappa = 1$, $N = 500$. *Top row.* Snapshots of u against the scaled particle index $\xi = \varepsilon j \in [0, 1]$, where the gray areas represent the intervals I_* and I_{**} from (1.15) as depicted in Figure 1.1. *Bottom row.* Evolution of the interface position Ξ as function of τ and snapshots of p against ξ with shaded area now indicating the interval J_* . *Interpretation.* In the macroscopic limit $\varepsilon \rightarrow 0$, a single phase interface propagates initially to the right but gets finally pinned at $\tau \approx 0.04$. Moreover, the scaled lattice data p approximate a macroscopic function P which is continuous everywhere and piecewise differentiable. On the microscopic scale, however, we find strong and localized fluctuations as illustrated in Figures 1.4 and 1.5.

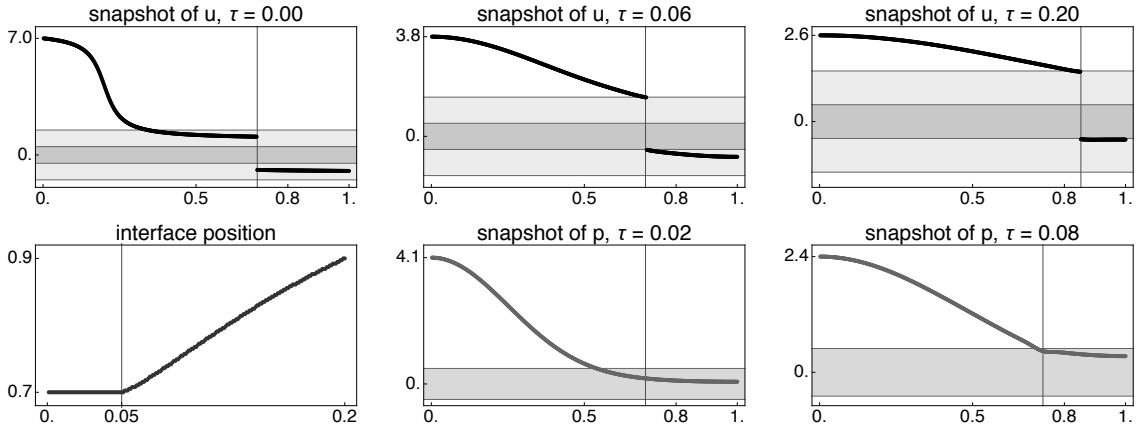


Figure 1.3: Second numerical example with depinning of the macroscopic interface at $\tau \approx 0.05$. On the moving interface, P attains the value $+p_*$ and $\partial_\xi P$ exhibits a jump, but when the interface rests, P is smooth across the interface with non-fixed value in J_* . This dichotomy gives rise to the hysteresis diagram in the right panel of Figure 1.1 and complies with both the Stefan condition (1.8) and the flow rule (1.10).

while $\Theta_0 := (-u_*, +u_*) = \{u : \Phi''(u) < 0\}$ is called the *spinodal region*. For the analysis of the macroscopic dynamics it is also convenient to introduce the intervals

$$I_* := [-u_*, +u_*], \quad I_{**} := [-u_{**}, +u_{**}], \quad J_* := [-p_*, +p_*], \quad (1.15)$$

where I_* and J_* are the closures of Θ_0 and $\Phi'(\Theta_0)$, respectively, and I_{**} denotes the inverse image of J_* under Φ' .

Numerical simulation as depicted in Figures 1.2 and 1.3 provide – for well prepared single-interface initial data as defined in Assumption 3.1 – evidence for the existence and dynamical stability of a macroscopic phase interface that separates two space-time regions in which the lattice data are confined to either one of the phases Θ_- and Θ_+ . The key observations concerning the corresponding large scale dynamics can be summarized as follows.

Observation 1.2 (Hysteretic flow rule on the macroscopic scale). *The macroscopic phase interface located at the curve $\xi = \Xi(\tau)$ can either propagate or be at rest according to the following rules:*

1. Standing interfaces: At any time τ with $\frac{d}{d\tau}\Xi(\tau) = 0$ we have $P(\tau, \Xi(\tau)) \in J_*$ and P is smooth across the interface.
2. Moving interfaces: $\frac{d}{d\tau}\Xi(\tau) \neq 0$ implies $P(\tau, \Xi(\tau)) = +p_*$ or $P(\tau, \Xi(\tau)) = -p_*$ depending on whether the interface propagates into the phase Θ_- or Θ_+ , respectively. The field P is still continuous across the interface but $\partial_\xi P$ admits a jump that drives the interface.

Moreover, continuity of P implies discontinuity for U and the type of each interface can change in time by pinning or depinning.

A closer look to the evolution of single particles – see Figures 1.4 and 1.5 – reveals the following features of the small scale dynamics.

Observation 1.3 (Phase transitions on the microscopic scale). *The microscopic dynamics of the phase interface are driven by particles u_j changing their phase as follows:*

1. Spinodal entrance: A particle u_j can enter the spinodal interval I_* only when its two neighbors belong to different phases and when one of these neighbors takes value outside of I_{**} . The microscopic phase interface therefore propagates on the lattice because the particles undergo a phase transition sequentially, that is, they pass through the spinodal interval I_* one after another.
2. Spinodal excursions: Not any spinodal visit is related to a proper phase transitions since it may happen that a particle enters and leaves the spinodal interval I_* on the same side.
3. Strong fluctuations Each spinodal visit (passage or excursion) evokes strong microscopic fluctuations that are initially very localized but in turn diffusively spread over the lattice.

Observations 1.2 and 1.3 match perfectly in that they relate the macroscopic speed of propagation to the number of particles that undergo a phase transition during a given period of time. In Proposition 2.2 we prove the crucial one-after-another-property in a simplified single-interface setting, and we obtain macroscopic Lipschitz estimates for the interface after bounding the asymptotic waiting time between adjacent phase transitions from below in Proposition 2.5 and Corollary 3.2.

The regularity observations that the macroscopic field P is continuous while the lattice data vary rapidly on the microscopic scale seem to contradict each other at first glance. The bridging idea is that macroscopic regularity can be observed in, loosely speaking, most of the macroscopic points (τ, ξ) while the rapid microscopic fluctuations with large amplitude dominate the dynamical behavior in a small subset of the macroscopic space-time only. These arguments are made rigorous in §3 and §4 where we prove that the superposition of all microscopic fluctuations converges as $\varepsilon \rightarrow 0$ pointwise almost everywhere to a continuous macroscopic field that drives the phase interface.

We also emphasize that Observation 1.3 combined with the trilinearity of Φ' allows us to decompose the nonlinear lattice (1.4) into linear subproblems as follows. As long as no particle is inside the spinodal region, the microscopic dynamics reduce – thanks to $\dot{u}_j = \dot{p}_j$ – to the discrete heat equation for p , and if some u_j is inside the spinodal region we can derive a linear equation for p where p_j diffuses backwards; see §3.1 for the details. Of course, the entire problem is still nonlinear since we have no a priori information about the spinodal entrance or exit times and hence do not know when to switch between the different linear evolutions. The linear decomposition is nonetheless very useful as it allows us to derive nearly explicit representation formulas for the lattice data in §3.

1.2 Multiple scales and fluctuations

The dynamics of the fluctuations are governed by a subtle interplay between the backward diffusion inside the spinodal region and the regularizing effects of the forward diffusion inside each phase. We can think of the fluctuations produced by the spinodal visit of some particle as a localized ‘package’ of fluctuations, which after its creation interacts by forward diffusion with the entire lattice and hence also with all packages evoked by former or later phase transitions. In particular, the ℓ^∞ -norm of

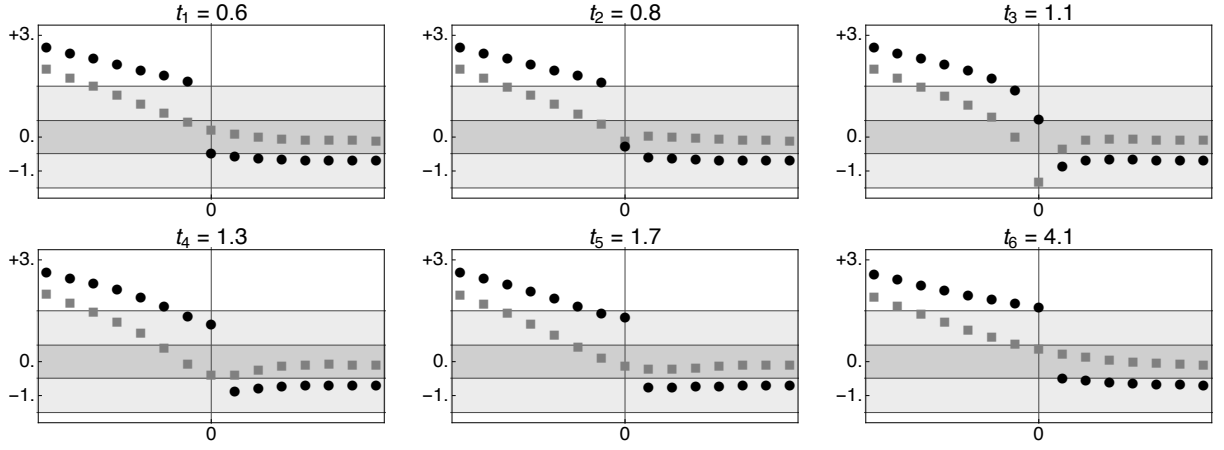


Figure 1.4: Snapshots of $u(t)$ (black points) and $p(t)$ (gray squares, affinely rescaled) against j at six non-equidistant times near the moving interface in a typical numerical simulation; the horizontal gray boxes illustrate again I_* and I_{**} . Particle u_0 passes the spinodal region I_* between the times t_1 and t_3 and creates strong fluctuations which are still localized at t_4 and not spread over lattice before t_5 . The next particle u_1 enters the spinodal region at time $t = t_6$.

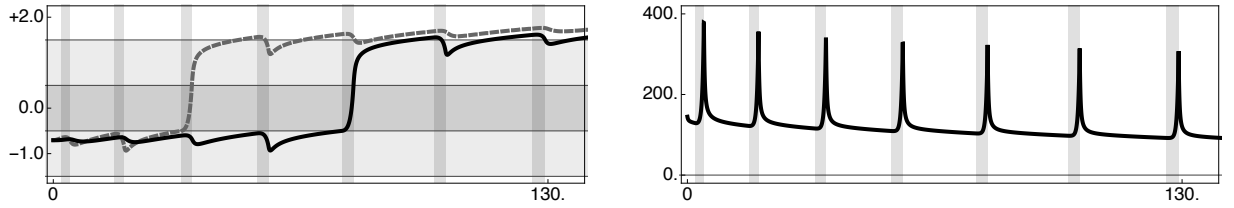


Figure 1.5: *Left panel.* Temporal trajectories of u_2 (gray, dashed) and u_4 (black, solid) for the numerical data from Figure 1.4. The k -th vertical boxes represents the spinodal passage of u_{k-1} during which fluctuations are created. *Right panel.* The evolution of the lattice dissipation \mathcal{D} from (1.16) with localized peak for each phase transition. In this numerical example we have $N = 200$ and relatively large initial dissipation $\mathcal{D}(0) \approx 140$, so the amplitude separation between peaks and bulk is rather small though clearly visible.

each package (amplitude) decays algebraically in time while the ℓ^1 -norm (mass) remains conserved since the fluctuations are not damped out but merely spread over the lattice. The microscopic lattice dynamics is therefore related to the informal concepts

1. *passage time* (time to pass the spinodal interval I_*),
2. *decay time* (time needed to spread and regularize the localized fluctuations),
3. *waiting time* (time between the phase transitions of adjacent particles),

and any mathematical analysis of the macroscopic limit $\varepsilon \rightarrow 0$ requires to understand the scaling relations of these times at least on a heuristic level.

We already mentioned that our asymptotic approach involves a precise lower bound for the waiting time as established for well-prepared initial data in Corollary 3.2. Moreover, in (3.12) we identify a universal *impact profile*, which provides the asymptotic shape of each package in the limit $\varepsilon \rightarrow 0$ and enables us in the proof of Lemma 3.10 to compute a microscopic time period of order ε^{-1} after which each package has been sufficiently regularized by the forward diffusion. This result can be regarded as an upper bound for the decay time although we state it differently and focus on the implied Hölder estimates for the regular fluctuations.

The heuristic concept of the passage time is a bit more involved. By splitting the microscopic dynamics during a spinodal passage into their slow and fast parts, we show in §3.1 that the *typical* passage time is of order $\ln \varepsilon$ due to the exponential growth of the fast variable. On the other hand, one can construct special initial data such that the first passage time is as large as the observation time. Even in this case, however, we can pass to the macroscopic limit since the interface does not move and because our results in §3.4 imply, roughly speaking, that the fluctuations remain localized

for all times and hence small with respect to macroscopic norms. By similar arguments we also control the cumulative impact of the spinodal excursion in Corollary 3.8 and do not attempt to estimate their number or duration.

The fluctuations as well as the different times scales can also be related to energetic concepts by regarding the lattice ODE (1.4) as gradient flow with respect to the spatially discrete analog to the H^{-1} -metric structure. In particular, for finite systems with either periodic or homogeneous Neumann boundary conditions we readily verify the energy law

$$\frac{d}{dt}\mathcal{E}(t) = -\varepsilon^2\mathcal{D}(t),$$

where

$$\mathcal{E}(t) := N^{-1} \sum_{j=1}^N \Phi(u_j), \quad \mathcal{D}(t) := N \sum_{j=1}^N (p_{j+1} - p_j)^2 \quad (1.16)$$

denote the *averaged energy* and the *dissipation*, respectively and both have been scaled such that the formal identification (1.7) complies with the macroscopic formulas

$$\mathcal{E}(t) \cong \int_0^1 \Phi(U(\varepsilon^2 t, \xi)) d\xi, \quad \mathcal{D}(t) \cong \int_0^1 (\partial_\xi P(\varepsilon^2 t, \xi))^2 d\xi.$$

Notice that the single-particle energy follows from (1.13) up to an additive constant and reads

$$\Phi(u) = \frac{1}{2} \begin{cases} (u+1)^2 & \text{if } u \leq -u_*, \\ (u-1)^2 & \text{if } u \geq +u_*, \\ p_* - \kappa u^2 & \text{if } -u_* < u < +u_*. \end{cases} \quad (1.17)$$

From (1.16) we infer for small $\varepsilon > 0$ the heuristic equivalence

$$\mathcal{D}(t) \sim 1 \quad \text{if and only if} \quad P(\varepsilon^2 t, \cdot) \text{ is regular with weak derivative } \partial_\xi P(\varepsilon^2 t, \cdot),$$

and conclude that the localized lattice fluctuations give rise to a significant increase in the dissipation. In other words, the interface dissipation stemming from microscopic phase transitions exceeds the regular dissipation coming from the macroscopic bulk diffusion. See the right panel in Figure 1.5 for typical numerical data and note that our asymptotic formulas ensure that $\mathcal{D}(t) \sim N = \varepsilon^{-1}$ at the end of each microscopic phase transition.

The energy equality for gradient flows

$$\int_0^\infty \mathcal{D}(\varepsilon^{-2}\tau) d\tau = \mathcal{E}(0) - \mathcal{E}(\infty),$$

reveals that the initial energy bounds the total number of microscopic phase transitions and hence also the maximal propagation distance of the macroscopic interface as well as the averaged impact of all fluctuations. It seems therefore tempting to tackle the macroscopic limit $\varepsilon \rightarrow 0$ by variational methods and to show that the gradient flow of the lattice Γ -converges to the hysteretic free boundary problem (1.1), (1.8) and (1.10) whose variational structure is described in [Vis06]. Such approaches have been exploited in other micro-to-macro transitions, see for instance [OR07, Ser11, BBMN12, MT12, PSV12, Bra14] for different frameworks, and are usually quite robust. It is, however, not clear to the authors whether variational methods are capable of resolving the complicate dynamical behavior of (1.4) with non-monotone dissipation and temporally varying regularity of the microscopic data.

We finally recall that the above heuristic discussion of the lattice dynamic is restricted to well-prepared macroscopic single-interface data. All arguments can be adapted to the case of finitely many

phase interfaces but other classes of initial data are more crucial. For instance, numerical simulations with oscillatory single-interface indicate the existence of an initial transient regime during which the systems dissipates a huge amount of energy before it reaches a state with macroscopic regularity for the first time. It seems, however, that there is no simple way to estimate the duration of the transient regime because a large number of phase transitions might push the phase interface over a long distance and produce many additional fluctuations. The dynamics of multi-phase initial data with oscillatory phase fraction or data with many particles inside the spinodal region are even more complicated since we expect to find measure-valued solutions on the macroscopic scale as well as phase interfaces that connect a pure-phase region with a mixed-phase one. First results in this direction have been obtained in [Hol16] for a bilinear nonlinearity and a periodic pattern for the microscopic phase field, but in the general case with an irregular distribution of phases it is not even clear what the analog to the hysteretic flow rule (1.10) is. Moreover, for arbitrary initial data there is an extra transient regime related to the spinodal decomposition of particles but it seems hard to show that the latter happens in a sufficiently short period of time.

1.3 Main result and plan of paper

In this paper we derive the hysteretic free boundary problem (1.1), (1.8) and (1.10) in the trilinear case (1.13) and for well-prepared single-interface initial data on the \mathbb{Z} . The prototypical example of the latter stems – as in Figures 1.2 and 1.3 – from a macroscopic initial datum with single interface located at $\xi = \Xi_{\text{ini}}$ and phases Θ_+ and Θ_- corresponding to $\xi < \Xi_{\text{ini}}$ and $\xi > \Xi_{\text{ini}}$, respectively. More precisely, after choosing a bounded, continuous, and piecewise smooth function P_{ini} on \mathbb{R} such that

$$P_{\text{ini}}(\xi) > -p_* \quad \text{for } \xi < \Xi_{\text{ini}}, \quad P_{\text{ini}}(\xi) \in J_* \quad \text{for } \xi > \Xi_{\text{ini}},$$

we consistently set

$$U_{\text{ini}}(\xi) := P_{\text{ini}}(\xi) + 1 \in \Theta_+ \quad \text{for } \xi < \Xi_{\text{ini}}, \quad U_{\text{ini}}(\xi) := P_{\text{ini}}(\xi) - 1 \in \Theta_- \cap I_{**} \quad \text{for } \xi > \Xi_{\text{ini}}$$

and initialize the lattice data by a discrete sampling via (1.7). Due to the upper bound $P_{\text{ini}}(\xi) \leq +p_*$ for $\xi > \Xi_{\text{ini}}$, the phase interface can propagate only to the right but it can switch between standing and moving by (several) pinning or depinning events.

For such initial data, the macroscopic model predicts a unique interface curve Ξ with phase field

$$M(\tau, \xi) = \text{sgn } U(\tau, \xi) = \text{sgn } (\Xi(\tau) - \xi) = U(\tau, \xi) - P(\tau, \xi)$$

as well as $\llbracket U \rrbracket = \llbracket P + M \rrbracket = \llbracket M \rrbracket = -2$ at $\xi = \Xi(\tau)$ and for all times $\tau \geq 0$. We can therefore eliminate both U and M in the limit problem and summarize our main findings as follows.

Main result 1.4 (Lattice data satisfy hysteretic Stefan problem). *For macroscopic single-interface initial data as described above, the scaled lattice data converge as $\varepsilon \rightarrow 0$ to a solution of the hysteretic free boundary problem. In particular, the limit consists of a macroscopic field P along with a nondecreasing interface curve $\Gamma = \{(\tau, \xi) : \xi = \Xi(\tau)\}$ such that the following equations are satisfied:*

$$\text{linear bulk diffusion outside } \Gamma : \quad \partial_\tau P = \partial_\xi^2 P \tag{1.18}$$

$$\text{Stefan condition across } \Gamma : \quad 2 \frac{d}{d\tau} \Xi = \llbracket \partial_\xi P \rrbracket \quad \text{and} \quad \llbracket P \rrbracket = 0 \tag{1.19}$$

$$\text{hysteretic flow rule on } \Gamma : \quad P = +p_* \text{ if } \frac{d\Xi}{d\tau} > 0 \quad \text{and} \quad \frac{d\Xi}{d\tau} = 0 \text{ if } P \in (-p_*, +p_*) \tag{1.20}$$

Moreover, Ξ and P are Lipschitz and locally Hölder continuous, respectively, and uniquely determined by Ξ_{ini} and P_{ini} .

The conditions on the initial data are made precise in Assumption 3.1, and the limit is established in several steps in §4. Proposition 4.1 first provides macroscopic compactness of the scaled lattice data and in Theorem 4.2 we verify the limit dynamics along convergent subsequences. Both the convergence and the uniqueness statement then follow because the Cauchy problem for (1.18), (1.19)

and (1.20) is well-posed, see [Vis06] and [MTT09] for approaches via hysteresis operators and entropy inequalities, respectively.

The paper is organized as follows. In §2 we prove well-posedness for microscopic single-interface solutions, derive a lower bound on the waiting time, and establish the entropy balances on the discrete level. §3 is the main analytical part of this paper and concerns the macroscopic impact of the microscopic fluctuations. First, studying a linear model problem for a spinodal visit in §3.1, we characterize the backward-diffusion inside the spinodal region as the interaction of a scalar unstable mode with infinitely many slowly varying variables (slow-fast splitting). Afterwards we identify in §3.2 and §3.3 the microscopic fluctuations produced by a single particle and separate their essential part from the negligible one, where the former is given by the universal impact profile and the latter can be estimated with the help of the slow variables from the model problem. In §3.4 and §3.5 we deal with the superposition of all fluctuations and prove Hölder estimates for the regular part of the essential fluctuation as well as vanishing bounds for their residual part and for the negligible fluctuations. In §4 we finally pass to the limit $\varepsilon \rightarrow 0$ and derive the Main Result 1.4. Since the spinodal effects are well-controlled by the fluctuation estimates from §3, the corresponding arguments are similar to those from [HH13] for the bilinear limiting case $\kappa = \infty$.

We emphasize that the results of §2 can be generalized to more general bistable nonlinearities while our analysis in §3 is intimately connected to the trilinearity of Φ' as it relies on linear substitute problems and the superposition principle. Moreover, for general nonlinearities it is not clear what the analog to the aforementioned slow-fast splitting is.

1.4 On the numerical simulations

To conclude this introduction we describe the numerical scheme that was used for the computation of the examples in Figures 1.2 and 1.3. Fixing a finite particle number N , we impose homogeneous Neumann boundary conditions

$$u_0 \equiv u_1, \quad u_{N+1} \equiv u_N$$

and prescribe the initial data by

$$u_j(0) = c_{\pm} + d_{\pm} \arctan(\varepsilon j + e_{\pm}) \quad \text{for } j \gtrless j_*$$

with $\varepsilon = 1/N$. Here, j_* denotes the initial position of the single interface and the constants c_{\pm} , d_{\pm} , and e_{\pm} have been chosen carefully for any example to produce illustrative results, see the snapshots for $\tau = 0$.

We solve the ODE analog to the lattice (1.4) by the explicit Euler scheme, which is easy to implement. Of course, the numerical time step size δt must be chosen sufficiently small and in accordance with the macroscopic CFL condition

$$\frac{\delta \tau}{\delta \xi^2} = \frac{\varepsilon^2 \delta t}{(\varepsilon \delta j)^2} = \delta t < \lambda_{\max},$$

where the largest eigenvalue λ_{\max} of the discrete Laplacian $-\Delta$ is basically independent of the system size N and can be computed by discrete Fourier transform.

The numerical properties of the Euler scheme have already been investigated in [LM12], and the authors there regard the onset of strong oscillations as a drawback of the discretization. They also propose a semi-implicit scheme for the time integration of (1.4), which is unconditionally stable but requires to monitor the spinodal entrance and exit times, as well as a numerical algorithm for the computation of two-phase solutions to the free boundary problem (1.18)–(1.20). The latter scheme provides approximate solutions without spatial and temporal fluctuations as it imposes microscopic transmission conditions at the interface which are derived from the macroscopic entropy inequalities (1.11).

The oscillations in the Euler scheme are caused by the spinodal visits of particles and correspond precisely to the fluctuations described above on the level of the lattice equation with continuous

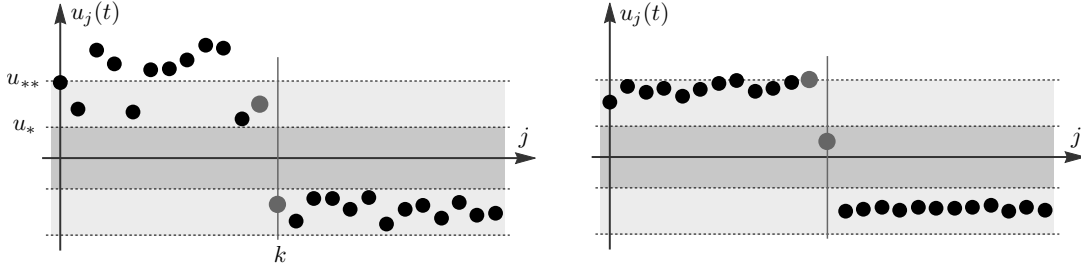


Figure 2.1: Two examples of single-interface states from X_k as in Definition 2.1, where u_{k-1} and u_k are highlighted. At the phase transition time t_k^* we have $u_k(t_k^*) = u_*$ as well as $\dot{u}_k(t_k^*) > 0$ according to Proposition 2.2 and the system moves into X_{k+1} .

time variable. Moreover, in view of the macroscopic free boundary problem one might in fact regard the microscopic oscillations as incorrect or spurious, but our analysis suggests a complementary interpretation. The fluctuations are the inevitable echo of the microscopic phase transitions, which drive the interface on large scales according to the hysteric flow rule (1.10) and explain why the thermodynamic fields comply with the entropy conditions (1.11) at all. In this context we emphasize that the solutions to the viscous approximation (1.3) also exhibit strong oscillations and one might argue that the rigorous passage to the limit $\varepsilon \rightarrow 0$ is still open because the fine structure of these oscillations has not yet been investigated carefully.

2 Properties of the lattice dynamics

In this section we investigate the dynamical properties of the diffusive lattice (1.4) with trilinear Φ' as in (1.13). All arguments, however, can be generalized to other bistable nonlinearities at the cost of more technical and notational efforts.

2.1 Existence of single-interface solutions

We first introduce the notion of single-interface solutions and establish their existence and uniqueness. Furthermore, we derive some basic properties concerning the dynamics of $p = \Phi'(u)$.

Definition 2.1 (Single-interface solution). *A differentiable function $u: [0, \infty) \rightarrow \ell^\infty(\mathbb{Z})$ is a single-interface solution to (1.4) if u satisfies the differential equation (1.4) and if there exists a non-decreasing sequence $(t_k^*)_{k \geq k_1} \subset (0, \infty]$, $k_1 \in \mathbb{Z}$ such that the following conditions are satisfied for all $k \geq k_1$ and with $t_{k_1-1}^* := 0$:*

1. *We have either $t_k^* = \infty$ or $t_{k+1}^* > t_k^*$.*
2. *If $t_{k-1}^* < \infty$, then u takes values in the state space*

$$X_k = \left\{ u \in \ell^\infty(\mathbb{Z}) : u_* < \inf_{j < k} u_j \leq \sup_{j < k} u_j < \infty, \quad -u_{**} < \inf_{j > k} u_j \leq \sup_{j > k} u_j < -u_*, \right. \\ \left. -u_{**} < u_k < u_* \right\}$$

on the time interval (t_{k-1}^, t_k^*) .*

If u is a single-interface solution with $u(t) \in X_k$ for some $k \in \mathbb{Z}$ and $t > 0$ then $u_j(t)$ belongs to the *positive phase* Θ_+ for $j < k$ and to the *negative phase* Θ_- for $j > k$, respectively; see Figure 2.1. At the *microscopic interface* $j = k$, however, $u_k(t)$ may be either in the negative phase or in the spinodal interval Θ_0 . Moreover, u_k may enter and leave the spinodal region via $u_k = -u_*$ several times during the dynamics of (1.4) in X_k , and we refer to the time intervals where $u_k \in \Theta_0$ as *spinodal visits* of u_k . On the other hand, the evolution continues in X_{k+1} once u_k passes through $u_k = +u_*$ at some *phase transition time* t_k^* .

The following proposition adapts [HH13, Theorem 3.2] to the present potential and provides the existence and uniqueness of single-interface solutions, where we assume from now on that $k_1 = 1$. The crucial argument is to show that the particles pass the spinodal region one after another. We derive this property in the framework of comparison principles but mention that a similar observation has been reported in [LM12].

Proposition 2.2 (Well-posedness of single-interface solutions). *For given initial data $u(0) \in X_1$ there exists a unique single-interface solution u to (1.4), and this solution satisfies*

$$-u_{**} \leq u_j(t) \leq \max\left(u_{**}, \sup_{j \in \mathbb{Z}} u_j(0)\right) \quad (2.1)$$

for all $t \geq 0$ and $j \in \mathbb{Z}$. Moreover, the entrance condition

$$u_k(t_k^*) = u_*, \quad \dot{u}_k(t_k^*) > 0 \quad \text{and} \quad t_{k+1}^* - t_k^* \geq C$$

holds for any $k \geq 1$ with $t_k^* < \infty$, where $C > 0$ depends only on Φ and the initial data, and the exit condition

$$u_{k-1}(t) > u_{**}, \quad (2.2)$$

holds at any time $t > 0$ with $u_k(t) = -u_*$ and $\dot{u}_k(t) \geq 0$.

Proof. Existence and uniqueness: The right hand side $\Delta \Phi'(\cdot)$ of (1.4) is Lipschitz continuous with respect to the ℓ^∞ -norm of u , so Picard's theorem yields the local existence and uniqueness of a continuously differentiable solution with values in $\ell^\infty(\mathbb{Z})$. Moreover, denoting the upper bound in (2.1) by D and introducing the state set

$$Y := \{u \in \ell^\infty : -u_{**} \leq u_j \leq D \text{ for all } j \in \mathbb{Z}\}$$

we infer from the properties of Φ' the implication

$$(u_j(t))_{j \in \mathbb{Z}} = Y \implies 2\Phi'(-u_{**}) \leq \dot{u}_j(t) + 2\Phi'(u_j(t)) \leq 2\Phi'(D) \text{ for all } j \in \mathbb{Z}.$$

The comparison principle for scalar ODEs reveals that Y is a forwardly invariant region for (1.4), and this ensures the global existence of solutions with (2.1).

Evolution in X_1 : For $u(t) \in X_1$ the dynamics of $p_j(t) = \Phi'(u_j(t))$ are governed by

$$\dot{p}_j(t) = \dot{u}_j(t) = \Delta p_j(t) \quad \text{for } j \neq 1,$$

and together with (2.1) we obtain

$$\begin{aligned} -2p_* &\leq \dot{p}_j(t) + 2p_j(t) \leq 2\Phi'(D) & \text{for } j < 1, \\ -2p_* &\leq \dot{p}_j(t) + 2p_j(t) \leq 2p_* & \text{for } j > 1. \end{aligned}$$

The comparison principle yields

$$\begin{aligned} p_j(t) &\geq -p_* (1 - e^{-2t}) + p_j(0)e^{-2t} & \text{for } j \neq 1, \\ p_j(t) &\leq +p_* (1 - e^{-2t}) + p_j(0)e^{-2t} & \text{for } j > 1 \end{aligned}$$

and from the continuity of u we infer that $u(t) \in X_1$ holds unless u_1 reaches either $-u_{**}$ or u_* . In addition, if $u_1(t)$ is not inside the spinodal region, that is if $u_1(t) < -u_*$, then we have $\dot{p}_1(t) \geq -2p_* - 2p_1(t)$ and this implies that $u_1(t)$ cannot reach $-u_{**}$. Hence, $u(t)$ either remains inside X_1 forever, which means $t_1^* := \infty$, or $u(t)$ reaches $\partial X_1 \cap \partial X_2$ at some time $t_1^* \in (0, \infty)$ with $u_1(t_1^*) = u_*$.

Spinodal exit and entrance condition: For $t_1^* < \infty$ we have

$$\dot{u}_1(t_1^*) = \Delta p_1(t_1^*) = p_0(t_1^*) + p_2(t_1^*) - 2(-p_*) > 0$$

since $p_j(t_1^*) > -p_*$ for $j \neq 1$, and we conclude that at the exit time t_1^* the solution u runs into X_2 with positive speed. Now suppose that $t \in (0, t_1^*)$ is an entrance time such that $u_1(t) = -u_*$ and $\dot{u}_1(t) \geq 0$. Then we compute

$$0 \leq \dot{u}_1(t) = p_0(t) + p_2(t) - 2p_* < p_0(t) - p_*$$

and obtain (2.2).

Lower bound for $t_2^* - t_1^*$: Repeating the two preceding steps in the case of $t_1^* < t_2^* < \infty$, we see that $u(t) \in X_2$ for $t \in (t_1^*, t_2^*)$, and that $p_1(t) > p_*$ holds at any entrance time with $u_2(t) = -u_*$ and $\dot{u}_2(t) \geq 0$. Moreover, for $t_2^* < \infty$ there exists a time $t_2^\# \in (t_1^*, t_2^*)$ such that $u_2(t_2^\#) = -u_*$ for the first time, and this implies

$$\dot{p}_1(t) = \Delta p_1(t) \leq \Phi'(D) + p_* - 2p_1(t) \quad \text{for } t \in (t_1^*, t_2^\#), \quad p_1(t_1^*) = -p_*, \quad p_1(t_2^\#) \geq +p_*.$$

The comparison principle for ODEs yields

$$p_* \leq p_1(t_2^\#) \leq \frac{1}{2}(\Phi'(D) + p_*)(1 - e^{-2(t_2^\# - t_1^*)}) - p_* e^{-2(t_2^\# - t_1^*)}$$

and after rearranging terms we obtain via

$$e^{2(t_2^* - t_1^*)} \geq e^{2(t_2^\# - t_1^*)} \geq \frac{\Phi'(D) + 3p_*}{\Phi'(D) - p_*} \quad (2.3)$$

a lower bound for $t_2^* - t_1^*$, where the above choice of D implies $\Phi'(D) \geq p_*$.

Conclusion: The proof can now be completed by iteration. \square

As an immediate consequence of Proposition 2.2 we obtain the following characterization of the dynamics of $p = \Phi'(u)$ which will be the starting point for our analysis of the spinodal fluctuations in §3.

Corollary 2.3 (Dynamics of $p = \Phi'(u)$). *Let u be a single-interface solution and denote by*

$$\chi_j(t) = 1 \quad \text{if } u_j(t) \in (-u_*, u_*), \quad \chi_j(t) = 0 \quad \text{otherwise} \quad (2.4)$$

the indicator of spinodal visits of u_j . Then $p_j = \Phi'(u_j)$ satisfies

$$\dot{p}_j(t) = (1 - \chi_j(t)) \Delta p_j(t) - \chi_j(t) \kappa \Delta p_j(t) \quad (2.5)$$

for all $j \in \mathbb{Z}$ and almost all $t > 0$.

Proof. Equation (2.5) is true for times t where $u_j(t) \notin \{\pm u_*\}$, because p_j is continuously differentiable in a neighborhood of such t and we have $\dot{p}_j(t) = \Phi''(u_j(t)) \Delta p_j(t)$ with either $\Phi''(u_j(t)) = 1$ or $\Phi''(u_j(t)) = -\kappa$. Moreover, the set of times $\{t: u_j(t) = +u_* \text{ for some } j \in \mathbb{Z}\}$ is by Proposition 2.2 contained in the countable set $\{t_k^*: k \in \mathbb{N}\}$ and thus not relevant for our discussion. The same is true for each set $T_j := \{t: u_j(t) = -u_*, \dot{u}_j(t) \neq 0\}$, which consists of isolated points and is hence also countable (it can be covered by disjoint open intervals, each of which containing a different rational number). It remains to consider $\mathcal{T}_j = \{t: u_j(t) = -u_*, \dot{u}_j(t) = 0\}$ with fixed $j \in \mathbb{Z}$. For any given $t \in \mathcal{T}_j$ and all sufficiently small $|h| > 0$ we observe that $u_j(t+h) = u_j(t) + \dot{u}_j(t)h + o(h) = -u_* + o(h)$ and find

$$|p_j(t+h) - p_j(t)| = |\Phi'(-u_* + o(h)) - \Phi'(-u_*)| \leq \max(1, \kappa) o(h).$$

This estimate implies $\dot{p}_j(t) = 0$, and combining this with $\Delta p_j(t) = \dot{u}_j(t) = 0$ we conclude that (2.5) is satisfied for all times in \mathcal{T}_j . \square

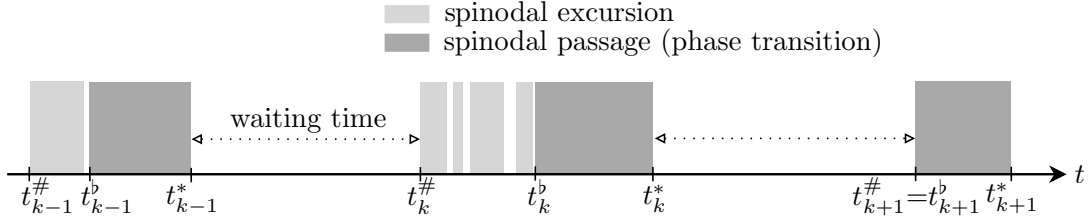


Figure 2.2: Schematic representation of the times from Notation 2.4. We control neither the number nor the duration of spinodal excursions but estimate their cumulative impact in Corollary 3.8.

2.2 Lower bound for the waiting time

Proposition 2.2 reveals the following dynamical properties for single-interface data:

1. at any time t there is at most one particle inside the spinodal region, and
2. the particles undergo their phase transition one after the other in the sense that u_{k+1} can enter the spinodal region only when u_k has completed its phase transition.

Our next goal is to show that the spinodal visits of neighboring particles are suitably separated. To this end we introduce the following times and refer to Figure 2.2 for an illustration.

Notation 2.4 (Spinodal entrance times, excursions and passage). Let u be a single-interface solution as in Proposition 2.2. For $k \geq 1$ we denote by

$$t_k^\# := \inf \{t > t_{k-1}^* : u_k(t) > -u_*\} \quad \text{and} \quad t_k^b := \inf \{t \geq t_k^\# : u_k(s) > -u_* \text{ for all } s > t\} \quad (2.6)$$

the *first* and the *final spinodal entrance time* of u_k , respectively. Moreover, we refer to spinodal visits of u_k that occur in $(t_k^\#, t_k^b)$ as *spinodal excursions* and to the spinodal visit in (t_k^b, t_k^*) as *spinodal passage*.

The quantity $t_{k+1}^\# - t_k^*$ is a lower bound for the difference $t_{k+1}^* - t_k^*$ between consecutive phase transition times and implies an upper bound for the microscopic interface speed. In the proof of Proposition 2.2, see (2.3), we have shown that $t_{k+1}^\# - t_k^* \geq C$ for some constant C , but this bound is not sufficient for passing to the macroscopic limit as it scales like $1/\varepsilon^2$ under the parabolic scaling (1.6). In the next lemma, we therefore derive an improved estimate for the difference $t_{k+1}^\# - t_k^*$ by means of problem-tailored comparison principles as sketched in Figure 2.3. To this end, we note that Proposition 2.2 combined with (1.14) implies for any $k \geq 1$ the estimates

$$-p_* \leq p_k(t) \leq p_* \quad \text{for } 0 \leq t \leq t_k^*, \quad -p_* \leq p_k(t) < \infty \quad \text{for } t \geq t_k^* \quad (2.7)$$

as well as

$$p_k(t_k^*) = -p_*, \quad p_k(t_{k+1}^\#) > +p_* = p_{k+1}(t_{k+1}^\#). \quad (2.8)$$

Moreover, we denote by g the discrete heat kernel, which solves

$$\dot{g}_j = \Delta g_j, \quad g_j(0) = \delta_j^0 \quad (2.9)$$

with Kronecker delta δ_j^0 and discrete Laplacian Δ as in (1.5). Notice that g can be computed explicitly by discrete Fourier transform, see for instance [HH13, Appendix].

Lemma 2.5 (Waiting Lemma). *Suppose there exists $b > 0$ such that the single-interface initial data $u(0) \in X_1$ satisfy*

$$p_j(0) \leq \gamma_j := p_* + b \max \{1 - j, 0\} \quad \text{for all } j \in \mathbb{Z}.$$

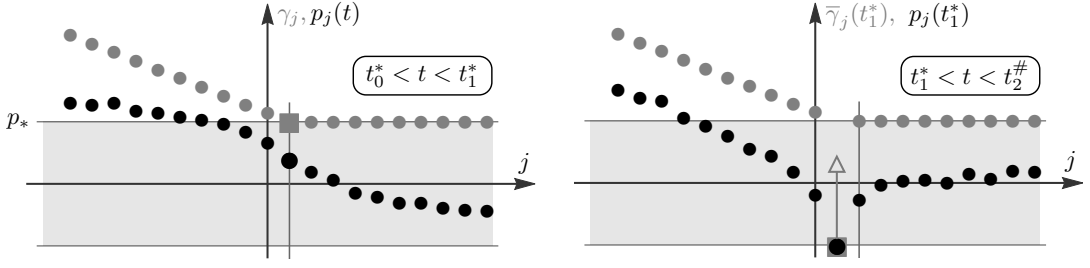


Figure 2.3: Illustration of Lemma 2.5 which provides a majorant for p and bounds the waiting time. *Left panel.* Cartoon of $p(t)$ (black) and the stationary, kink-type supersolution γ (gray) for $k = 1$ and times $t \in [t_0^*, t_1^*]$. At the phase transition time t_1^* , both the interface (vertical line) and γ are shifted to the right by one lattice position. *Right panel.* Cartoon of $p(t_1^*)$ and $\bar{\gamma}(t_1^*)$ for $k = 1$, where the time-dependent supersolution $\bar{\gamma}$ is used to estimate $t_2^\# - t_1^*$ from below. Notice that the phase interface has already been shifted to $j = 2$ and that Proposition 2.2 yields the two key conditions $p_1(t_1^*) = -p_*$ and $p_1(t_2^\#) > +p_*$.

Then the solution u from Proposition 2.2 satisfies

$$p_j(t) \leq \gamma_{j-k+1} \quad \text{for } j \in \mathbb{Z} \text{ and } t \in [t_{k-1}^*, t_k^*) \quad (2.10)$$

as well as

$$t_{k+1}^* - t_k^* \geq t_{k+1}^\# - t_k^* \geq \frac{c_* p_*}{b} \quad (2.11)$$

for all $k \geq 1$. Here, the universal constant c_* is determined by the discrete heat kernel, and (2.11) makes sense for $t_k^* < \infty$ only.

Proof. Supersolution for p in $[t_{k-1}^*, t_k^*]$: We start with $k = 1$ and suppose for contradiction that there exists a finite time $\tilde{t}_1 \in (t_0^*, t_1^*]$ such that

$$0 < \tilde{C} := \sup_{t \in [t_0^*, \tilde{t}_1]} \sup_{j \in \mathbb{Z}} c_j(t), \quad c_j(t) := p_j(t) - \gamma_j,$$

where $\tilde{C} \in \mathbb{R}$ is well-defined due to (2.1) and $t_0^* = 0$ holds by definition. By (2.7) we have

$$c_1(t) \leq p_* - \gamma_1 = 0 \quad \text{for } t_0^* \leq t \leq \tilde{t}_1, \quad (2.12)$$

while for $j \neq 1$ our definitions imply

$$\dot{c}_j = \dot{p}_j = \Delta p_j = \Delta c_j = c_{j+1} + c_{j-1} - 2c_j \leq 2(\tilde{C} - c_j)$$

thanks to Corollary 2.3. Therefore, and due to the initial condition $c_j(t_0^*) \leq 0$, the comparison principle for ODEs guarantees that

$$c_j(t) \leq \tilde{C}(1 - e^{-2t}) \quad \text{for } j \neq 1 \text{ and } t_0^* \leq t \leq \tilde{t}_1. \quad (2.13)$$

The combination of (2.12) and (2.13) finally yields $0 < \tilde{C} \leq \tilde{C}(1 - e^{-2\tilde{t}_1}) < \tilde{C}$ and hence the desired contradiction. In particular, we established the claim (2.10) for $k = 1$, and since this implies $p_j(t_1^*) \leq \gamma_j \leq \gamma_{j-1}$ we can proceed iteratively.

Estimate for $t_{k+1}^\# - t_k^*$: Due to the shift invariance it suffices again to study the case $k = 1$. As illustrated in Figure 2.3, we introduce $\bar{\gamma}$ as the solution to the initial value problem

$$\dot{\bar{\gamma}}_j(t) = \Delta \bar{\gamma}_j(t), \quad \bar{\gamma}_j(t_1^*) = \gamma_j - 2p_* \delta_j^1 \quad \text{for } j \in \mathbb{Z} \text{ and } t \geq t_1^*,$$

and using the discrete heat kernel g from (2.9) we write its explicit solution as

$$\bar{\gamma}_j(t) = \sum_{n \in \mathbb{Z}} g_{j-n}(t - t_1^*) \bar{\gamma}_n(t_1^*) = -2p_* g_{j-1}(t - t_1^*) + \sum_{n \in \mathbb{Z}} g_n(t - t_1^*) \gamma_{j-n}.$$

By differentiation of $\bar{\gamma}_1$ and recalling that

$$\sum_n \dot{g}_n(s) \gamma_{1-n} = \sum_n \Delta g_n(s) \gamma_{1-n} = \sum_n g_n(s) \Delta \gamma_{1-n} = b \sum_n g_n(s) \delta_n^0 = b g_0(s),$$

we find $\dot{\bar{\gamma}}_1(t) = -2p_* \dot{g}_0(t - t_1^*) + b g_0(t - t_1^*)$, which yields

$$\bar{\gamma}_1(t) = p_* - 2p_* g_0(t - t_1^*) + b \int_0^{t-t_1^*} g_0(s) ds$$

by integration and due to the initial conditions $\bar{\gamma}_1(t_1^*) = -p_*$, $g_0(0) = 1$. Since g_0 is positive and decreasing we conclude the existence of a unique time $\bar{t}_1 > t_1^*$ such that

$$\bar{\gamma}_1(\bar{t}_1) = p_* \quad \text{and} \quad \bar{\gamma}_1(t) < p_* \quad \text{for all } t \in [t_1^*, \bar{t}_1], \quad (2.14)$$

and exploiting $g_0(s) \sim (1+s)^{-1/2}$ we justify that

$$\bar{t}_1 - t_1^* \geq \frac{c_* p_*}{b} \quad (2.15)$$

holds for some universal constant $c_* > 0$. Moreover, p solves the discrete heat equation for $t \in [t_1^*, t_2^\#]$, where we have

$$p_j(t_1^*) \leq \bar{\gamma}_j(t_1^*) \quad \text{for all } j \in \mathbb{Z}$$

according to (2.10) and since $p_1(t_1^*) = -p_*$ holds by (2.8). A standard comparison principle therefore yields

$$p_j(t) \leq \bar{\gamma}_j(t) \quad \text{for all } j \in \mathbb{Z} \text{ and } t \in [t_1^*, t_2^\#],$$

and in combination with (2.14) we obtain $t_2^\# > \bar{t}_1$ since (2.8) also guarantees that $p_1(t_2^\#) \geq p^*$. The desired estimate (2.11) now follows from (2.15). \square

2.3 Family of entropy inequalities

We finally establish the discrete analog to the weak formulation of the entropy relation (1.11) as well as the local variant of the energy-dissipation relation.

Proposition 2.6 (Entropy balance and energy dissipation). *Let $\psi \in \ell^1(\mathbb{Z})$ be an arbitrary but nonnegative test function, $t \geq 0$ a given time, and u be a solution to (1.4). Then we have*

$$\frac{d}{dt} \sum_{j \in \mathbb{Z}} \eta(u_j(t)) \psi_j \leq - \sum_{j \in \mathbb{Z}} \mu(p_j(t)) (\nabla_+ \psi_j) (\nabla_+ p_j(t)) \quad (2.16)$$

for any smooth entropy pair (η, μ) satisfying (1.12) as well as

$$\sum_{j \in \mathbb{Z}} \int_0^t (\nabla_+ p_j(s))^2 \psi_j ds \leq \sum_{j \in \mathbb{Z}} \Phi(u_j(0)) - \sum_{j \in \mathbb{Z}} \int_0^t p_j(s) (\nabla_+ \psi_j) (\nabla_+ p_j(s)) ds \quad (2.17)$$

with energy Φ as in (1.17).

Proof. Since (1.12) ensures $\frac{d}{dt} \eta(u_j) = \eta'(u_j) \dot{u}_j = \mu(p_j) \Delta p_j$, we compute

$$\begin{aligned} \frac{d}{dt} \sum_{j \in \mathbb{Z}} \eta(u_j) \psi_j &= \sum_{j \in \mathbb{Z}} \psi_j \mu(p_j) \nabla_- \nabla_+ p_j = - \sum_{j \in \mathbb{Z}} \nabla_+ (\psi_j \mu(p_j)) \nabla_+ p_j \\ &= - \sum_{j \in \mathbb{Z}} \mu(p_j) \nabla_+ \psi_j \nabla_+ p_j - \sum_{j \in \mathbb{Z}} \psi_{j+1} \nabla_+ \mu(p_j) \nabla_+ p_j, \end{aligned} \quad (2.18)$$

where we used discrete integration by parts as well as the product rule $(a_{j+1} b_{j+1} - a_j b_j) = b_j(a_{j+1} - a_j) + a_{j+1}(b_{j+1} - b_j)$. The monotonicity of μ implies

$$\nabla_+ \mu(p_j) \nabla_+ p_j = (\mu(p_{j+1}) - \mu(p_j))(p_{j+1} - p_j) \geq 0,$$

so (2.16) follows immediately thanks to the nonnegativity of ψ . Moreover, choosing $(\eta, \mu) = (\Phi, \text{id})$ and integrating (2.18) in time we obtain (2.17) after rearranging terms and due to $\Phi(u_j(t)) \geq 0$. \square

3 Analysis of the spinodal fluctuations

As already discussed in §1, the analysis of the fluctuations is the very core of the convergence problem and so far we are only able to deal with trilinear nonlinearities Φ' because for those we can decompose the nonlinear dynamics into linear subproblems and combine all partial results by the superposition principle. We also recall that the case $\kappa \in (0, \infty)$ is more involved than the bilinear limit $\kappa = \infty$ without spinodal excursions and with degenerate spinodal passages.

The asymptotic arguments below strongly rely on the regularity of the microscopic initial data. To keep the presentation as simple as possible we make from now on the following standing assumption, which guarantees that the initial data are well-prepared.

Assumption 3.1 (Macroscopic single-interface initial data). *The initial data $u(0)$ belong to X_1 and there exist constants $\alpha, \beta > 0$ such that $p(0) = \Phi'(u(0)) = u(0) - \text{sgn } u(0)$ satisfies*

$$\sup_{j \in \mathbb{Z}} |p_j(0)| \leq \alpha, \quad \sup_{j \in \mathbb{Z}} |\nabla_+ p_j(0)| \leq \alpha \varepsilon, \quad \sup_{j \in \mathbb{Z} \setminus \{1\}} |\Delta p_j(0)| \leq \alpha \varepsilon^2$$

as well as

$$|\Delta p_1(0)| \leq \beta \varepsilon, \quad p_j(0) \leq p_* + \varepsilon \beta \max\{0, 1 - j\} \quad \text{for all } j \in \mathbb{Z}$$

for $\varepsilon > 0$. Moreover, for convenience we assume that $u_1(0) \notin (-u_*, +u_*)$.

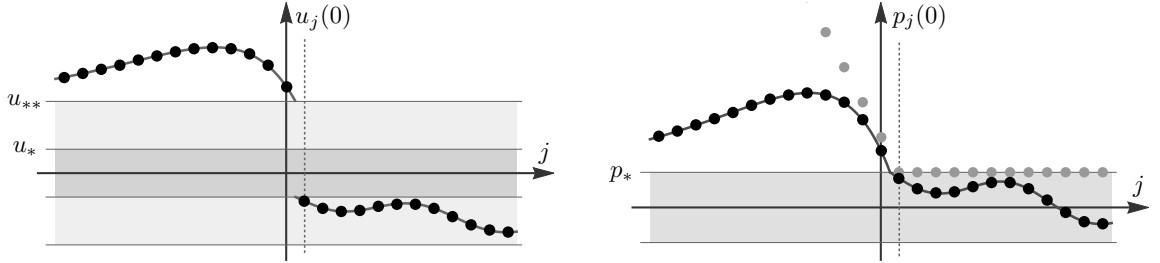


Figure 3.1: Typical initial data (black dots) as in Assumption 3.1 which sample macroscopic functions U_{ini} and $P_{\text{ini}} = U_{\text{ini}} - \text{sgn } U_{\text{ini}}$ (gray curves) that are compatible with the limit model from Main Result 1.4. The gray dots represent the kink-type majorant for $p(0)$ which enables us to bound all microscopic waiting times from below and hence the macroscopic interface speed from above, see Lemma 2.5 and Corollary 3.2.

Assumption 3.1 is motivated by the limit dynamics, see Figure 3.1 for an illustration, and the prototypical example from §1.3 corresponds to $\Xi_{\text{ini}} = 0$ and

$$\alpha = \sup_{\xi \in \mathbb{R}} (|P_{\text{ini}}(\xi)| + |P'_{\text{ini}}(\xi)| + |P''_{\text{ini}}(\xi)|), \quad \beta = \max \left\{ \|\partial_\xi P_{\text{ini}}(\Xi_{\text{ini}})\|, \sup_{\xi < \Xi_{\text{ini}}} ((P_{\text{ini}}(\xi) - p_*)/\xi) \right\}.$$

An important consequence of Assumption 3.1 and Lemma 2.5 are the following bounds for the microscopic waiting time and the number of microscopic phase transitions.

Corollary 3.2 (Waiting Lemma for macroscopic single-interface initial data). *The microscopic single-interface solution from Proposition 2.2 satisfies*

$$t_{k+1}^* - t_k^* \geq t_{k+1}^\# - t_k^* \geq \frac{2d_*}{\varepsilon}$$

for all $k \geq 1$ with $t_k^* < \infty$ and some constant $d_* > 0$, which depends only on the potential parameter κ and on the initial data via the parameters α, β . In particular, for any macroscopic final time $\tau_{\text{fin}} > 0$ we have

$$K_\varepsilon := \max\{k \geq 1 : t_k^* \leq \tau_{\text{fin}}/\varepsilon^2\} \leq \frac{\tau_{\text{fin}}}{2d_*\varepsilon},$$

where K_ε abbreviates the number of phase transitions in the corresponding microscopic time interval $[0, t_{\text{fin}}]$ with $t_{\text{fin}} := \tau_{\text{fin}}/\varepsilon^2$.

Notation 3.3 (Generic constants and parameter dependence). In the following, we always suppose that $0 < \tau_{\text{fin}} < \infty$ is fixed and denote by C a generic constant that depends on κ, α, β , and τ_{fin} but not on $\varepsilon > 0$.

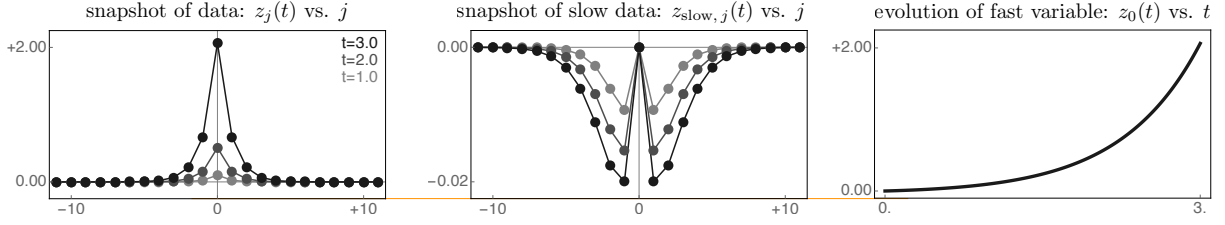


Figure 3.2: Solution to the spinodal problem (3.1) with $\kappa = 1$, vanishing initial data, and source term $f(t) \equiv 0.02$. Due to the backward diffusion of z_0 , *all* lattice data z_j change rapidly in time and explode exponentially but the slow variables from Lemma 3.4 behave much nicer.

3.1 Prototypical spinodal problem

Equation (2.5) reveals that during a spinodal visit of some u_k the corresponding $p_k = \Phi'(u_k)$ satisfies $\dot{p}_k = -\kappa \Delta p_k$ while all other p_j adhere to forward diffusion $\dot{p}_j = \Delta p_j$. For this reason, we first consider a prototypical spinodal problem

$$\dot{z}_j(t) = \begin{cases} -\kappa \Delta z_0(t) + (1 + \kappa)f(t) & \text{if } j = 0, \\ +\Delta z_j(t) & \text{if } j \neq 0, \end{cases} \quad \text{for } j \in \mathbb{Z}, t \geq 0, \quad (3.1)$$

where z represents some part of p and where f is a perturbation whose purpose will become clear later. Given bounded initial data at time $t = 0$, the ODE (3.1) admits a unique solution, and our goal in this section is to understand how the backward diffusing z_0 interacts with the forward diffusing background and the source term $(1 + \kappa)f$. A typical numerical simulation is shown in Figure 3.2.

Splitting the solution z into its even and odd parts according to

$$z_{\text{even},j}(t) := \frac{1}{2}(z_{+j}(t) + z_{-j}(t)) \quad \text{and} \quad z_{\text{odd},j}(t) := \frac{1}{2}(z_{+j}(t) - z_{-j}(t)),$$

respectively, we first observe that z_{even} also satisfies (3.1), whereas z_{odd} solves the discrete heat equation. Next, introducing the variables

$$\zeta_n(t) = \frac{1+2\kappa}{2\kappa} z_{\text{even},n}(t) - \frac{1}{2\kappa} z_{\text{even},n-1}(t), \quad n \geq 1 \quad (3.2)$$

we verify by direct computation the identities

$$\dot{z}_0(t) = \frac{(2\kappa)^2}{1+2\kappa} (z_0(t) - \zeta_1(t)) + (1 + \kappa)f(t) \quad (3.3)$$

and

$$\dot{\zeta}_n(t) = \begin{cases} \zeta_2(t) - \zeta_1(t) - \frac{1+\kappa}{2\kappa} f(t) & \text{if } n = 1, \\ \Delta \zeta_n & \text{if } n > 1. \end{cases}$$

The key observation is that ζ solves the discrete heat equation on the semi-infinite domain $n \geq 1$ with inhomogeneous Neumann boundary condition at $n = 1$. Therefore, if the initial data $z(0)$ and the source term $f(t)$ are uniformly small in j and t , respectively, then all components of ζ evolve *slowly*, and the same is true for z_{odd} as well. On the other hand, the *fast* variable z_0 exhibits a strong tendency to grow exponentially and changes generically by an order 1 in times of order 1. In this sense, the change of variables

$$z \in \ell^1(\mathbb{Z}) \quad \rightsquigarrow \quad (z_0, z_{\text{odd}}, \zeta) \in \mathbb{R} \times \ell^1(\mathbb{N}) \times \ell^1(\mathbb{N})$$

separates the slow and fast dynamics of (3.1) and allows us to isolate a single ‘unstable mode’ as follows.

Lemma 3.4 (Slow-fast splitting for the prototypical phase-transition problem). *Any solution to (3.1) can be written as*

$$z_j(t) = z_{\text{fast},j}(t) + z_{\text{slow},j}(t) \quad \text{with} \quad z_{\text{fast},j}(t) := \frac{z_0(t)}{(1 + 2\kappa)^{|j|}}, \quad z_{\text{slow}} := z - z_{\text{fast}},$$

and we have

$$\sum_{j \in \mathbb{Z}} |z_{\text{slow},j}(t)| \leq C \left(\sum_{j \in \mathbb{Z}} |z_j(0)| + \int_0^t |f(s)| \, ds \right)$$

for some constant C which depends only on the parameter κ .

Proof. Parity splitting and odd solutions: In view of the even-odd parity of the prototypical phase-transition model (3.1) it suffices to consider solutions that are either even or odd. For odd initial data, we always have $z_j(t) = -z_{-j}(t)$ and the assertions follow with

$$z_{\text{fast},j}(t) = 0, \quad z_{\text{slow},j}(t) = z_j(t) = z_{\text{odd},j}(t)$$

since z satisfies the discrete heat equation.

Even solutions: Using $z_j(t) = z_{\text{even},j}(t)$ as well as the definition of ζ in (3.2) we verify the representation formula

$$z_{-j}(t) = z_j(t) = \frac{z_0(t)}{(1+2\kappa)^j} + \frac{2\kappa}{(1+2\kappa)^{j+1}} \sum_{n=1}^j (1+2\kappa)^n \zeta_n(t) \quad \text{for all } j \geq 1,$$

where the first and the second term on the right hand side represent z_{fast} and z_{slow} , respectively. In particular, we estimate

$$\begin{aligned} \sum_{j \in \mathbb{Z}} |z_{\text{slow},j}(t)| &\leq \sum_{j=1}^{\infty} \frac{4\kappa}{(1+2\kappa)^{j+1}} \sum_{n=1}^j (1+2\kappa)^n |\zeta_n(t)| \\ &= \sum_{n=1}^{\infty} |\zeta_n(t)| \sum_{j=n}^{\infty} \frac{4\kappa}{(1+2\kappa)^{j-n+1}} = 2 \sum_{n=1}^{\infty} |\zeta_n(t)| \end{aligned}$$

for all $t \geq 0$. Next, an off-site reflection with respect to $j = 1/2$, that is,

$$\tilde{\zeta}_j(t) = \begin{cases} \zeta_j(t) & \text{if } j \geq 1, \\ \zeta_{1-j}(t) & \text{if } j \leq 0, \end{cases}$$

transforms the boundary value problem for ζ into the discrete diffusion system

$$\frac{d}{dt} \tilde{\zeta}_j(t) = \Delta \tilde{\zeta}_j(t) - (\delta_j^0 + \delta_j^1) \frac{1+\kappa}{2\kappa} f(t) \quad \text{for all } j \in \mathbb{Z} \quad \text{and } t \geq 0$$

with source term at $j = 0$ and $j = 1$. Duhamel's Principle gives

$$\zeta_j(t) = \tilde{\zeta}_j(t) = \sum_{n \in \mathbb{Z}} g_{j-n}(t) \tilde{\zeta}_n(0) - \int_0^t (g_j(t-s) + g_{j-1}(t-s)) \frac{1+\kappa}{2\kappa} f(s) \, ds$$

for all $j \geq 1$, and the claim follows from

$$\sum_{j \in \mathbb{Z}} |\tilde{\zeta}_j(0)| \leq C \sum_{j \in \mathbb{Z}} |z_j(0)|$$

and the mass conservation property of the discrete heat kernel. \square

The proof of Lemma 3.4 is intimately related to the linearity of the spinodal problem (3.1) as it allows us to construct the slow variables explicitly. For a general bistable nonlinearity, it remains a challenging task to identify the analog to (3.2) and (3.3). We also mention that the existence of a single unstable mode has been shown in [LM12] for a finite dimensional analog to (3.1) using spectral analysis of tridiagonal matrices. It has also been argued that spinodal passages are typically fast with respect to the diffusive time scale. Lemma 3.4 extends these results to unbounded domains and quantifies the asymptotic slowness of the stable modes in a robust and reliable way.

3.2 Spinodal fluctuations

As indicated in the previous section, we think of spinodal fluctuations as unstable modes in an otherwise diffusive evolution, which are evoked by spinodal visits of the u_j 's or, equivalently, by the linear backward diffusion of the corresponding p_j 's. To study this systematically, we define the k -th spinodal fluctuation $r^{(k)} := (r_j^{(k)})_{j \in \mathbb{Z}}$ to be

$$r_j^{(k)}(t) := \begin{cases} 0 & \text{for } 0 \leq t \leq t_k^\#, \\ -p_j(t) + q_j^{(k)}(t) & \text{for } t_k^\# \leq t \leq t_k^*, \\ \sum_{n \in \mathbb{Z}} g_{j-n}(t - t_k^*) r_n^{(k)}(t_k^*) & \text{for } t_k^* < t, \end{cases} \quad (3.4)$$

where g is the discrete heat kernel from (2.9) and

$$q_j^{(k)}(t) := \begin{cases} 0 & \text{for } t < t_k^\#, \\ \sum_{n \in \mathbb{Z}} g_{j-n}(t - t_k^\#) p_n(t_k^\#) & \text{for } t > t_k^\# \end{cases} \quad (3.5)$$

solves the discrete heat equation for $t > t_k^\#$ with initial data $p(t_k^\#)$.

Formula (3.4) is at the heart of our asymptotic analysis and enables us to characterize both the local and the global behavior of the fluctuations. On the local side, we infer from (3.4) and Corollary 2.3 that the evolution of each $r^{(k)}$ is determined by the initial condition

$$r_j^{(k)}(t_k^\#) = 0 \quad \text{for all } j \in \mathbb{Z} \quad (3.6)$$

as well as the equations

$$\dot{r}_j^{(k)}(t) = \begin{cases} (1 - \chi_k(t)) \Delta r_k^{(k)}(t) + \chi_k(t) \left(-\kappa \Delta r_k^{(k)}(t) + (1 + \kappa) \dot{q}_k^{(k)}(t) \right) & \text{if } j = k, \\ \Delta r_j^{(k)}(t) & \text{if } j \neq k \end{cases} \quad (3.7)$$

for almost every $t \in (t_k^\#, t_k^*)$ and

$$\dot{r}_j^{(k)}(t) = \Delta r_j^{(k)}(t), \quad j \in \mathbb{Z} \quad (3.8)$$

for $t > t_k^*$, where the indicator function χ_k has been introduced in (2.4). In particular, $r^{(k)}(t)$ satisfies – at any time t with $\chi_k(t) = 1$ and hence on the entire interval $(t_k^\#, t_k^*)$ – a shifted and delayed variant of the prototypical phase transition problem (3.1) with forcing term $\dot{q}_k^{(k)}(t)$, and this gives rise to the local fluctuation estimates in §3.3. On the other hand, arguing recursively we derive from (3.4) and (3.5) the representation formula

$$p_j(t) = \sum_{n \in \mathbb{Z}} g_{j-n}(t) p_j(0) - \sum_{k \geq 1} r_j^{(k)}(t) \quad \text{for all } j \in \mathbb{Z} \text{ and } t \geq 0, \quad (3.9)$$

where the first and the second sum on the right hand side account for the initial data and the cumulative impact of all phase transitions, respectively. This identity allows us in §3.4 to sheave the local fluctuation estimates into global ones and to quantify how much p deviates from the diffusive reference data due to the spinodal visits of all particles. Finally, since p and $q^{(k)}$ are uniformly bounded due to (2.1) and (3.5), the maximum principle for the discrete heat equation guarantees

$$\sup_{k \geq 1} \sup_{j \in \mathbb{Z}} \sup_{t \geq 0} |r_j^{(k)}(t)| \leq C, \quad (3.10)$$

where the constant C depends only on the potential Φ and the initial data $p(0)$.

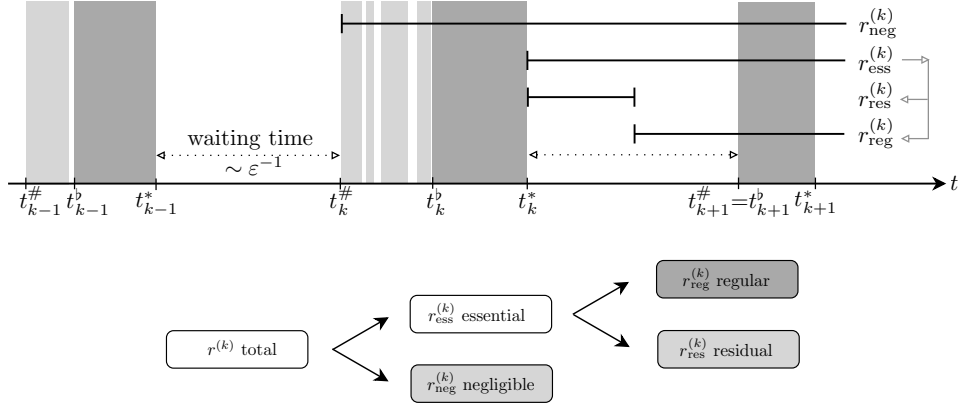


Figure 3.3: Life span of the total fluctuations (3.4) and their parts defined in (3.19), (3.20) and (3.27). Both the negligible and the residual fluctuations vanish in the macroscopic limit, see Corollary 3.8 and Lemma 3.9, while the sum of all regular fluctuations drives the interface in the free boundary problem as shown in §4.2.

The remainder of §3 deals with the analysis of the spinodal fluctuations. As indicated in Figure 3.3, it turns out that spinodal excursions and the spinodal passage of a u_k lead to two distinguishable parts of $r^{(k)}$, namely the *negligible fluctuations* $r_{\text{neg}}^{(k)}$ and the *essential fluctuations* $r_{\text{ess}}^{(k)}$, respectively. We will show that the negligible fluctuations are not relevant for the macroscopic dynamics, whereas the essential fluctuations contribute significantly to them. More precisely, $r_{\text{ess}}^{(k)}$ can be split further into a *regular* part, which leads to a sufficiently regular limit contribution, and a *residual* part which vanishes in suitable function spaces, see the proof of Proposition 4.1 below.

We finally emphasize that phase transitions in the bilinear case $\kappa = \infty$ are instantaneous processes since the spinodal region has shrunk to a point. In particular, at the phase transition time $t_k^* = t_k^\#$, the value of u_k is continuous but changes its sign from negative to positive while p_k is discontinuous as it jumps down from $+p^*$ to $-p^*$. We therefore have

$$r_j^{(k)}(t_k^* + 0) = r_{\text{ess},j}^{(k)}(t_k^* + 0) = 2p_* \delta_j^k \quad \text{for} \quad \kappa = \infty$$

and no negligible fluctuations at all.

3.3 Local fluctuation estimates

In the next two lemmas, we study the fluctuations $r^{(k)}$ for a fixed $k \geq 1$, and a key quantity for the analysis is

$$D_k := \int_{t_k^\#}^{t_k^*} |\dot{q}_k^{(k)}(s)| \, ds, \quad (3.11)$$

which allows us to bound the source term in (3.7). Specifically, employing a slow-fast splitting as in §3.1 we characterize the fluctuations induced by u_k at the end of its phase transition and show that these are – up to small error terms – given by a shifted variant of the universal *impact profile* ϱ with

$$\varrho_j := \frac{2p_*}{(1 + 2\kappa)|j|}, \quad (3.12)$$

which depends only on κ and is illustrated in Figure 3.4. Notice that the definition of p_* in (1.14) ensures $\sum_{j \in \mathbb{Z}} \varrho_j = 2$ for all $\kappa \in (0, \infty)$ as well as $\varrho_j = 2\delta_j^0$ for $\kappa = \infty$ and $\varrho_j \rightarrow 0$ pointwise as $\kappa \rightarrow 0$.

Lemma 3.5 (Estimates for spinodal excursions of u_k). *For any $k \geq 1$ we have*

$$\sup_{t \in [t_k^\#, t_k^b]} \sum_{j \in \mathbb{Z}} |r_j^{(k)}(t)| \leq C(1 + D_k) \quad (3.13)$$

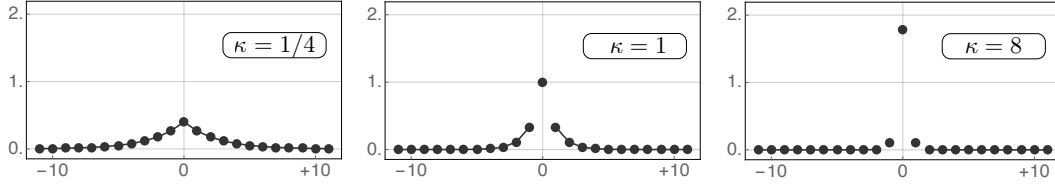


Figure 3.4: The impact profile ϱ from (3.12) as function of j for several values of the spinodal parameter κ . The essential fluctuations produced by each microscopic phase transition are given by a shifted and delayed variant of $g * \varrho$, see (3.18) and (3.19), and contribute to the driving force of the macroscopic phase interface.

as well as

$$\sum_{j \in \mathbb{Z}} |r_j^{(k)}(t_k^\flat)| \leq CD_k \quad (3.14)$$

for some constant $C > 0$ and spinodal entrance times $t_k^\#$, t_k^\flat as in (2.6).

Proof. Throughout the proof we drop the upper index k to ease the notation. Equation (3.7) can be written as

$$\dot{r}_j(t) = \Delta r_j(t) + \delta_j^k \chi_k(t) \frac{1 + \kappa}{\kappa} (\dot{r}_k(t) - \dot{q}_k(t))$$

for $t \in (t_k^\#, t_k^\flat)$, and using discrete integration by parts we find

$$\begin{aligned} \frac{d}{dt} \sum_{j \in \mathbb{Z}} |r_j(t)| &= \sum_{j \in \mathbb{Z}} \operatorname{sgn} r_j(t) \Delta r_j(t) + \operatorname{sgn} r_k(t) \chi_k(t) \frac{1 + \kappa}{\kappa} (\dot{r}_k(t) - \dot{q}_k(t)) \\ &= - \sum_{j \in \mathbb{Z}} \nabla_+ \operatorname{sgn} r_j(t) \nabla_+ r_j(t) + \operatorname{sgn} r_k(t) \chi_k(t) \frac{1 + \kappa}{\kappa} (\dot{r}_k(t) - \dot{q}_k(t)) \\ &\leq C \left(\frac{d}{dt} |r_k(t)| + |\dot{q}_k(t)| \right), \end{aligned} \quad (3.15)$$

where we used the monotonicity of the sign function. Thanks to (3.6), the fluctuations r vanish at time $t_k^\#$, so an integration yields

$$\sum_{j \in \mathbb{Z}} |r_j(t)| \leq C |r_k(t)| + C \int_{t_k^\#}^t |\dot{q}_k(s)| ds \quad (3.16)$$

for all $t \in [t_k^\#, t_k^\flat]$, and this proves (3.13) due to the bound (3.10). Moreover, by

$$q_k(t_k^\#) = p_k(t_k^\#) = p_k(t_k^\flat) = p_*$$

we have

$$|r_k(t_k^\flat)| = |q_k(t_k^\flat) - p_*| \leq \int_{t_k^\#}^{t_k^\flat} |\dot{q}_k(s)| ds + |q_k(t_k^\#) - p_*| \leq D_k + 0$$

and obtain (3.14) as a further consequence of (3.16). \square

Lemma 3.6 (Estimates for the spinodal passage of u_k). *For any $k \geq 1$ we have*

$$\sup_{t \in [t_k^\flat, t_k^*]} \sum_{j \in \mathbb{Z}} |r_j^{(k)}(t)| \leq C(1 + D_k) \quad (3.17)$$

as well as

$$\sum_{j \in \mathbb{Z}} \left| r_j^{(k)}(t_k^*) - \varrho_{j-k} \right| \leq CD_k \quad (3.18)$$

for some constant C .

Proof. The proof of (3.17) is identical to the one of (3.13) in the previous lemma because (3.15) is also true for $t \in [t_k^\#, t_k^*]$. To derive (3.18) let us consider times $t \in (t_k^b, t_k^*)$, so that u_k is located inside the spinodal region and (3.7) can be written as

$$\dot{r}_j(t) = \begin{cases} -\kappa \Delta r_k(t) + (1 + \kappa) \dot{q}_k(t) & \text{if } j = k, \\ +\Delta r_j(t) & \text{if } j \neq k, \end{cases}$$

where we dropped the upper index k for simplicity of notation. After shifting time and space by t_k^b and k , respectively, this is the prototypical phase transition problem (3.1) with $z = r$ and $f = \dot{q}$, and from Lemma 3.4 we obtain

$$\sum_{j \in \mathbb{Z}} \left| r_j(t) - \frac{r_k(t)}{(1 + 2\kappa)^{|j-k|}} \right| \leq C \left(\sum_{j \in \mathbb{Z}} |r_j(t_k^b)| + \int_{t_k^b}^t |\dot{q}_k(s)| ds \right) \leq CD_k,$$

where the second inequality is due to (3.14) and (3.11). The claim (3.18) now follows because $p_k(t_k^*) = -p_*$ and $q_k(t_k^\#) = p_*$ provide

$$|r_k(t_k^*) - 2p_*| = |q_k(t_k^*) - p_*| \leq \int_{t_k^\#}^{t_k^*} |\dot{q}(s)| ds + |q_k(t_k^\#) - p_*| \leq D_k + 0$$

and since $\sum_{j \in \mathbb{Z}} \varrho_j$ is finite. \square

For small D_k we infer from (3.18) that at the end of the spinodal passage of u_k the induced fluctuations $r^{(k)}(t_k^*)$ are in fact close to the shifted impact profile from (3.12). This observation together with the definition of $r^{(k)}(t)$ for $t > t_k^*$ – see (3.4), (3.7), and (3.8) – motivates the splitting of $r^{(k)}$ into an *essential* part

$$r_{\text{ess},j}^{(k)}(t) := \chi_{\{t \geq t_k^*\}} \sum_{n \in \mathbb{Z}} g_{j-n}(t - t_k^*) \varrho_{n-k} \quad (3.19)$$

and the remainder

$$r_{\text{neg},j}^{(k)} := r_j^{(k)}(t) - r_{\text{ess},j}^{(k)}(t), \quad (3.20)$$

which we call the *negligible* fluctuations. We prove in §3.4 below that these names are justified since Assumption 3.1 implies that $r_{\text{ess}}^{(k)}$ is relevant for the limit dynamics, whereas $r_{\text{neg}}^{(k)}$ is not.

Notice also that Lemma 3.5 and Lemma 3.6 are again intimately related to the trilinearity of Φ' . It remains open to identify more robust proof strategies that cover general bistable nonlinearities as well and provide the analog to the impact profile (3.12) and the splitting (3.19)–(3.20) for a broader class of nonlinear lattices (1.4).

3.4 Global fluctuation estimates

In view of §3.3, the main technical task for collectively controlling the fluctuations for all $k \geq 1$ is to estimate the sum of the quantities D_k from (3.11). Our starting point is the representation formula

$$q_j^{(k)}(t) = \sum_{n \in \mathbb{Z}} g_{j-n}(t) p_n(0) - \sum_{l=1}^{k-1} \sum_{n \in \mathbb{Z}} g_{j-n}(t - t_l^*) r_n^{(l)}(t_l^*) \quad \text{for all } j \in \mathbb{Z} \text{ and } t \geq t_k^\#, \quad (3.21)$$

which follows from (3.4) and (3.5) by induction over k and splits $q^{(k)}$ into one part stemming from the initial data and another one from the previous phase transitions.

Lemma 3.7 (Upper bound for D_k). *There exists a constant C such that*

$$\sum_{k=1}^{K_\varepsilon} D_k \leq \frac{C}{\sqrt{\varepsilon}}$$

for all sufficiently small $\varepsilon > 0$.

Proof. By (3.21) we have

$$\dot{q}_k^{(k)}(t) = \sum_{n \in \mathbb{N}} \dot{g}_{k-n}(t) p_n(0) - \sum_{l=1}^{k-1} \sum_{n \in \mathbb{Z}} \dot{g}_{k-n}(t - t_l^*) r_n^{(l)}(t_l^*) \quad (3.22)$$

for all $t \in (t_k^\#, t_k^*)$, and due to Assumption 3.1 we can estimate the contribution from the initial data by

$$\left| \sum_{n \in \mathbb{Z}} \dot{g}_{k-n}(t) p_n(0) \right| = \left| \sum_{n \in \mathbb{Z}} g_{k-n}(t) \Delta p_n(0) \right| \leq C \left(\alpha \varepsilon^2 + \frac{\beta \varepsilon}{(1+t)^{1/2}} \right)$$

because the discrete heat kernel g from (2.9) is nonnegative and satisfies $\sum_{j \in \mathbb{Z}} g_j(t) = 1$ as well as $\sup_{j \in \mathbb{Z}} g_j(t) \leq C(1+t)^{-1/2}$. Moreover, the contributions from the previous phase transitions $l = 1, \dots, k-1$ satisfy

$$\left| \sum_{n \in \mathbb{Z}} \dot{g}_{k-n}(t - t_l^*) r_n^{(l)}(t_l^*) \right| \leq \|\dot{g}(t - t_l^*)\|_{\ell^\infty} \sum_{n \in \mathbb{Z}} |r_n^{(l)}(t_l^*)| \leq C \frac{1 + D_l}{(1 + t - t_l^*)^{3/2}}$$

thanks to Lemma 3.6 and $\|\dot{g}_j(s)\|_{\ell^\infty} \leq -\dot{g}_0(s) \leq C/(1+s)^{3/2}$. Combining these estimates with (3.11) and integrating (3.22) we thus find

$$D_k \leq \int_{t_k^\#}^{t_k^*} \alpha \varepsilon^2 + \frac{\beta \varepsilon}{(1+t)^{1/2}} dt + C \sum_{l=1}^{k-1} \int_{t_k^\#}^{t_k^*} \frac{1 + D_l}{(1 + t - t_l^*)^{3/2}} dt. \quad (3.23)$$

Summing over all phase transitions in $[0, t_{\text{fin}}]$, we estimate the first integral in (3.23) by

$$\sum_{k=1}^{K_\varepsilon} \int_{t_k^\#}^{t_k^*} \alpha \varepsilon^2 + \frac{\beta \varepsilon}{(1+t)^{1/2}} dt \leq \int_0^{t_{\text{fin}}} \alpha \varepsilon^2 + \frac{\beta \varepsilon}{(1+t)^{1/2}} dt \leq \alpha \tau_{\text{fin}} + 2\beta \sqrt{\varepsilon^2 + \tau_{\text{fin}}} \leq C \quad (3.24)$$

and the second one by

$$\begin{aligned} \sum_{k=1}^{K_\varepsilon} \sum_{l=1}^{k-1} \int_{t_k^\#}^{t_k^*} \frac{1 + D_l}{(1 + t - t_l^*)^{3/2}} dt &= \sum_{l=1}^{K_\varepsilon} (1 + D_l) \sum_{k=l+1}^{K_\varepsilon} \int_{t_k^\#}^{t_k^*} \frac{dt}{(1 + t - t_l^*)^{3/2}} \\ &\leq \sum_{l=1}^{K_\varepsilon} (1 + D_l) \int_{t_{l+1}^\#}^{\infty} \frac{dt}{(1 + t - t_l^*)^{3/2}} \\ &\leq 2 \sum_{l=1}^{K_\varepsilon} \frac{1 + D_l}{(1 + t_{l+1}^\# - t_l^*)^{1/2}}. \end{aligned} \quad (3.25)$$

Moreover, Corollary 3.2 provides $(1 + t_{l+1}^\# - t_l^*)^{-1/2} \leq C\sqrt{\varepsilon}$. Adding the partial estimates (3.24) and (3.25) we thus arrive at

$$\sum_{k=1}^{K_\varepsilon} D_k \leq C \left(1 + \sqrt{\varepsilon} K_\varepsilon + \sqrt{\varepsilon} \sum_{k=1}^{K_\varepsilon} D_k \right),$$

and the thesis follows by rearranging terms since Corollary 3.2 ensures that $K_\varepsilon \leq C/\varepsilon$. \square

As a consequence of Lemma 3.7, we obtain an upper bound for the sum of all negligible fluctuations.

Corollary 3.8 (Uniform ℓ^1 -bound for all negligible fluctuations). *We have*

$$\sup_{0 \leq t \leq t_{\text{fin}}} \sum_{j \in \mathbb{Z}} \sum_{k=1}^{K_\varepsilon} |r_{\text{neg},j}^{(k)}(t)| \leq \frac{C}{\sqrt{\varepsilon}} \quad (3.26)$$

for some constant C and all sufficiently small $\varepsilon > 0$.

Proof. Fix $t \in [0, t_{\text{fin}}]$ and note that if $t \leq t_1^\#$ then there are no fluctuations at all and the claim is trivially true at t . Otherwise the single-interface property from Proposition 2.2 provides exactly one $l \in \{1, \dots, K_\varepsilon\}$ such that

$$\text{either } t \in [t_l^\#, t_l^*) \quad \text{or} \quad t \in [t_l^*, t_{l+1}^\#),$$

where $t_{K_\varepsilon+1}^\#$ may be larger than t_{fin} or even infinite. In the first case we have

$$r_{\text{neg}}^{(l)}(t) = r^{(l)}(t), \quad r_{\text{neg}}^{(k)}(t) = 0 \quad \text{for } k > l$$

according to the definitions in (3.19) and (3.20), and using the local fluctuation estimates from Lemmas 3.5 and 3.6 we find

$$\begin{aligned} \sum_{j \in \mathbb{Z}} \sum_{k=1}^{K_\varepsilon} |r_{\text{neg},j}^{(k)}(t)| &\leq \sum_{j \in \mathbb{Z}} |r_{\text{neg},j}^{(l)}(t)| + \sum_{j \in \mathbb{Z}} \sum_{k=1}^{l-1} |r_{\text{neg},j}^{(k)}(t)| = \sum_{j \in \mathbb{Z}} |r_j^{(l)}(t)| + \sum_{j \in \mathbb{Z}} \sum_{k=1}^{l-1} |r_j^{(k)}(t) - r_{\text{ess},j}^{(k)}(t)| \\ &\leq C(1 + D_l) + \sum_{j \in \mathbb{Z}} \sum_{k=1}^{l-1} \sum_{n \in \mathbb{Z}} g_{j-n}(t - t_k^*) \left| r_n^{(k)}(t_k^*) - \varrho_{n-k} \right| \\ &\leq C(1 + D_l) + C \sum_{k=1}^{l-1} D_k. \end{aligned}$$

The discussion of the second case $t \in [t_l^*, t_{l+1}^\#)$ is even simpler since the contributions for $k = l$ and $k < l$ can be bounded in the same way. In particular, arguing as above we find

$$\sum_{j \in \mathbb{Z}} \sum_{k=1}^{K_\varepsilon} |r_{\text{neg},j}^{(k)}(t)| \leq \sum_{j \in \mathbb{Z}} \sum_{k=1}^l |r_j^{(k)}(t) - r_{\text{ess},j}^{(k)}(t)| \leq C \sum_{k=1}^l D_k,$$

and the claim follows in both cases from Lemma 3.7. \square

Notice that the superposition of all essential fluctuations satisfies

$$\sum_{j \in \mathbb{Z}} \sum_{k=1}^{K_\varepsilon} r_{\text{ess},j}^{(k)}(t) = 2 \max \{k : t_k^* \leq t\}$$

since we have $\sum_{j \in \mathbb{Z}} \varrho_j = 2$ and because the convolution with the discrete heat kernel g preserves mass as well as positivity. Consequently, the sum of all essential fluctuations is of order $1/\varepsilon$ and hence larger than the right hand side in (3.26), provided that the interface propagates on the macroscopic scale. In other words, the negligible fluctuations are in fact smaller than the essential ones.

We further emphasize that we are not able to estimate the number of spinodal excursions or their duration. Corollary 3.8, however, controls the impact of the corresponding fluctuations even in the worst-case-scenario that a single particle is either always inside the spinodal region or enters and leaves it repeatedly over a very long period of time. More precisely, combining the estimate (3.26) with the scaling (1.6) we show in §4.1 that the sum of all negligible fluctuations is small in the macroscopic L^1 -norm and confirm in this way that spinodal excursions are not related to proper phase transitions and do not drive the interface in the macroscopic free boundary problem (1.18)–(1.20).

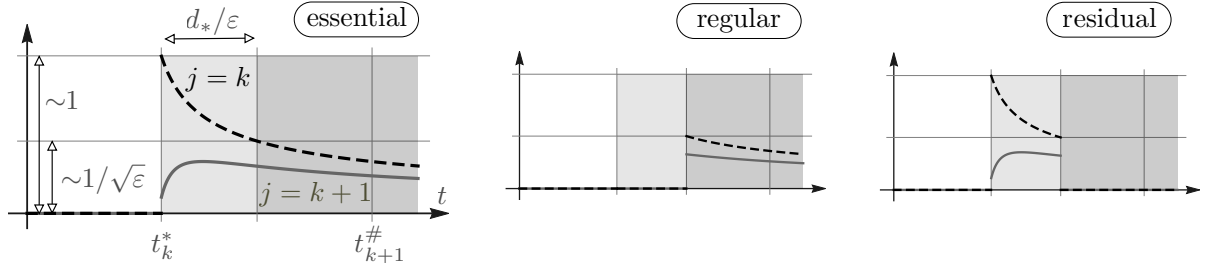


Figure 3.5: Cartoon of the essential fluctuations $r_{\text{ess},j}^{(k)}$ and the corresponding regular and residual ones, see (3.27), depicted as functions of t for $j = k$ (black, dashed) and $j = k + 1$ (gray, solid). The shaded boxes indicate the different life spans.

3.5 Regularity of fluctuations

A fundamental ingredient for passing to the macroscopic limit in §4 is to ensure that the superposition of all fluctuations converges to a continuous function. The essential fluctuations $r_{\text{ess},k}^{(k)}$, however, are discontinuous in time as they jump at every t_k^* , see Figure 3.5. To overcome this problem we observe that the lower bound for the waiting time guarantees that the diffusion effectively regularizes $r_{\text{ess}}^{(k)}$ in the time between t_k^* and $t_{k+1}^\#$. We therefore split the latter into two parts and denote by

$$r_{\text{reg},j}^{(k)}(t) := r_{\text{ess},j}^{(k)}(t)\chi_{[t_k^*, t_k^* + d_*/\varepsilon]}(t) \quad \text{and} \quad r_{\text{res},j}^{(k)}(t) := r_{\text{ess},j}^{(k)}(t)\chi_{[t_k^* + d_*/\varepsilon, t_{k+1}^\#]}(t) \quad (3.27)$$

the k -th *regular* and *residual* fluctuations, respectively, where d_* is the constant from Corollary 3.2. The regular fluctuations are still discontinuous in time but it turns out that the jumps are small and disappear as $\varepsilon \rightarrow 0$. On the other hand, the sum of all residual fluctuations is very irregular but the Lebesgue measure of its domain of definition becomes small under the scaling (1.6).

Lemma 3.9 (Uniform ℓ^1 -bound for residual fluctuations). *We have*

$$\sup_{0 \leq t \leq t_{\text{fin}}} \sum_{j \in \mathbb{Z}} \sum_{k=1}^{K_\varepsilon} |r_{\text{res},j}^{(k)}(t)| \leq C$$

for some constant C and all sufficiently small $\varepsilon > 0$.

Proof. By Corollary 3.2 the intervals $[t_k^*, t_k^* + d_*/\varepsilon]$ are mutually disjoint and we conclude that for any t only one k contributes to the double sum. Combining this with (3.19), (3.27) and the mass conservation of the discrete heat equation we find

$$\sum_{j \in \mathbb{Z}} \sum_{k=1}^{K_\varepsilon} |r_{\text{res},j}^{(k)}(t)| = \sup_{1 \leq k \leq K_\varepsilon} \sum_{j \in \mathbb{Z}} |r_{\text{res},j}^{(k)}(t)| \leq C$$

with $C := \sum_{j \in \mathbb{Z}} \varrho_j$. □

The key result of this section is the following lemma, which shows that the regular fluctuations are Hölder continuous up to a small error that vanishes in the limit $\varepsilon \rightarrow 0$.

Lemma 3.10 (Hölder estimates for regular fluctuations). *There exists a constant C , which depends on κ and d_* such that*

$$\left| \sum_{k=1}^{K_\varepsilon} r_{\text{reg},j_2}^{(k)}(t_2) - \sum_{k=1}^{K_\varepsilon} r_{\text{reg},j_1}^{(k)}(t_1) \right| \leq C\varepsilon^{1/2} \left(|t_2 - t_1|^{1/4} + |j_2 - j_1|^{1/2} \right) + C\varepsilon^{1/2} \quad (3.28)$$

holds for any $j_1, j_2 \in \mathbb{Z}$ and all $0 \leq t_1, t_2 \leq t_{\text{fin}}$.

Proof. Elementary arguments reveal that the discrete heat kernel satisfies

$$|g_{j_2}(t_2) - g_{j_1}(t_1)| \leq \frac{C}{(1 + \min\{t_1, t_2\})^{3/4}} (|t_2 - t_1|^{1/4} + |j_2 - j_1|^{1/2}), \quad (3.29)$$

see for instance [HH13, Appendix] for the details. In what follows we denote the argument of the modulus on left hand side of (3.28) by $D(t_1, t_2, j_1, j_2)$ and study the cases $j_1 = j_2$ and $t_1 = t_2$ separately. The general result is then a consequence of the triangle inequality.

Spatial regularity: For $t_1 = t_2 = t$, inequality (3.29) along with (3.19) and (3.27) implies

$$\begin{aligned} |D(t, t, j_1, j_2)| &\leq \sum_{k: t_k^* \leq t - d_*/\varepsilon} \sum_{n \in \mathbb{Z}} \varrho_{n-k} |g_{j_2-n}(t - t_k^*) - g_{j_1-n}(t - t_k^*)| \\ &\leq C |j_2 - j_1|^{1/2} \sum_{k: t_k^* \leq t - d_*/\varepsilon} \frac{1}{(1 + t - t_k^*)^{3/4}} \end{aligned}$$

with ϱ as in (3.12). Moreover, the lower bound for the waiting time in Corollary 3.2 guarantees that all phase transition times are sufficiently separated from each other, and hence also that

$$\#\{k : t_k^* < t - d_*/\varepsilon\} \leq \left\lfloor \frac{\varepsilon t}{2d_*} \right\rfloor,$$

where $\lfloor \cdot \rfloor$ denotes the floor function. As illustrated in Figure 3.6, we can therefore estimate

$$\sum_{k: t_k^* \leq t - d_*/\varepsilon} \frac{1}{(1 + t - t_k^*)^{3/4}} \leq C \sum_{l=1}^{\lfloor \varepsilon t / (2d_*) \rfloor} \left(\frac{\varepsilon}{ld_*} \right)^{3/4} = C \varepsilon t^{1/4} \leq C \tau_{\text{fin}}^{1/4} \varepsilon^{1/2} \leq C \varepsilon^{1/2}, \quad (3.30)$$

where we interpreted the sum as a discretized Riemann integral, and obtain via

$$|D(t, t, j_1, j_2)| \leq C \varepsilon^{1/2} |j_2 - j_1|^{1/2},$$

the claim (3.28) in the first case.

Temporal regularity: Supposing $j_1 = j_2 = j$ and $t_1 < t_2$, we write

$$D(t_1, t_2, j, j) = D_1(t_1, t_2, j) + D_2(t_1, t_2, j),$$

where

$$D_1(t_1, t_2, j) = \sum_{k: t_k^* + d_*/\varepsilon < t_1} \sum_{n \in \mathbb{Z}} \varrho_{n-k} (g_{j-n}(t_2 - t_k^*) - g_{j-n}(t_1 - t_k^*))$$

and

$$D_2(t_1, t_2, j) = \sum_{k: t_1 \leq t_k^* + d_*/\varepsilon < t_2} \sum_{n \in \mathbb{Z}} \varrho_{n-k} g_{j-n}(t_2 - t_k^*)$$

account for the phase transitions that occur in the intervals $[0, t_1]$ and $[t_1, t_2]$, respectively. To estimate the first term, we employ (3.29) and Corollary 3.2 as in the above discussion and infer that

$$|D_1(t_1, t_2, j)| \leq C |t_2 - t_1|^{1/4} \sum_{k: t_k^* + d_*/\varepsilon < t_1} \frac{1}{(1 + t_1 - t_k^*)^{3/4}} \leq C \varepsilon^{1/2} |t_2 - t_1|^{1/4}.$$

Moreover, the decay $g_j(t) \leq C/(1+t)^{1/2}$ for all $j \in \mathbb{Z}$ and $t \geq 0$ yields

$$|D_2(t_1, t_2, j)| \leq \sum_{k: t_1 \leq t_k^* + d_*/\varepsilon < t_2} \frac{C}{(1 + t_2 - t_k^*)^{1/2}},$$

and Corollary 3.2 combined with $|t_2 - t_1| \leq t_{\text{fin}} = \tau_{\text{fin}}/\varepsilon^2$ allows us to estimate

$$\begin{aligned} |D_2(t_1, t_2, j)| &\leq \sum_{l=1}^{\lceil \varepsilon(t_2 - t_1)/(2d_*) \rceil} \frac{C \varepsilon^{1/2}}{(ld_*)^{1/2}} \\ &\leq C \varepsilon |t_2 - t_1|^{1/2} + C \varepsilon^{1/2} \leq C \varepsilon^{1/2} |t_2 - t_1|^{1/4} + C \varepsilon^{1/2}, \end{aligned}$$

where $\lceil \cdot \rceil$ denotes the ceiling function. □

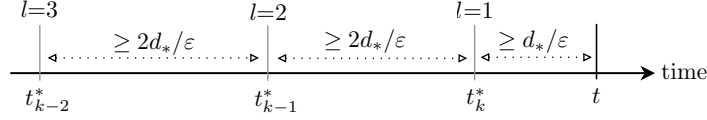


Figure 3.6: To control the regularity of the fluctuations in the proof of Lemma 3.10, we look from a given time t backward and label the past phase transitions in reversed order by the index l .

As a consequence of Lemma 3.10 we obtain the following bound for the regular fluctuations.

Corollary 3.11 (ℓ^∞ -bound for all fluctuations). *There exists a constant C such that*

$$\sup_{t \in [0, t_{\text{fin}}]} \sup_{j \in \mathbb{Z}} \left(\left| \sum_{k=1}^{K_\varepsilon} r_{\text{reg},j}^{(k)}(t) \right| + \left| \sum_{k=1}^{K_\varepsilon} r_{\text{res},j}^{(k)}(t) \right| + \left| \sum_{k=1}^{K_\varepsilon} r_{\text{neg},j}^{(k)}(t) \right| \right) \leq C$$

for all sufficiently small $\varepsilon > 0$.

Proof. The claimed estimate for the residual fluctuations is a direct consequence of Lemma 3.9 while the bound for the regular fluctuations follows from Lemma 3.10 with $t_2 = t$, $t_1 = 0$, $j_1 = j_2 = j$ and due to $t^{1/4} \leq t_{\text{fin}}^{1/4} = \tau_{\text{fin}}^{1/4} \varepsilon^{-1/2}$. Moreover, the representation formula (3.9) implies

$$\sup_{t \in [0, t_{\text{fin}}]} \sup_{j \in \mathbb{Z}} \left| \sum_{k=1}^{K_\varepsilon} r_j^{(k)}(t) \right| \leq C$$

thanks to Proposition 2.2, Assumption 3.1, and the maximum principle for diffusion equations. The assertion for the negligible fluctuations thus follows from $r_{\text{neg},j}^{(k)}(t) = r^{(k)}(t) - r_{\text{reg},j}^{(k)}(t) - r_{\text{res},j}^{(k)}(t)$, which is provided by (3.19), (3.20), and (3.27). \square

We conclude this section with an estimate for the spatial gradient of the regular fluctuations. To begin with, setting $j_1 = j$, $j_2 = j + 1$ and $t_1 = t_2 = t$ in (3.28) provides

$$\left| \sum_{k=1}^{K_\varepsilon} \nabla_+ r_{\text{reg},j}^{(k)}(t) \right| \leq C \varepsilon^{1/2},$$

so the corresponding macroscopic gradient is bounded pointwise in space and time by $\varepsilon^{-1/2}$ but not by some quantity of order 1. The following result, however, establishes an improved ℓ^2 -estimate which enables us to pass to the macroscopic limit pointwise in time.

Lemma 3.12 (ℓ^2 -bound for the gradient of regular fluctuations). *We have*

$$\sup_{0 \leq t \leq t_{\text{fin}}} \sum_{j \in \mathbb{Z}} \left| \sum_{k=1}^{K_\varepsilon} \nabla_+ r_{\text{reg},j}^{(k)}(t) \right|^2 \leq C \varepsilon$$

for some constant C and all sufficiently small $\varepsilon > 0$.

Proof. The gradient of the discrete heat kernel satisfies

$$\sum_{j \in \mathbb{Z}} |\nabla_+ g_j(t)|^2 \leq C(1+t)^{-3/2},$$

for all $t \geq 0$, see for instance [HH13, Appendix], and (3.19), (3.27) ensure

$$\nabla_+ r_{\text{reg},j}^{(k)}(t) = \sum_{n \in \mathbb{Z}} \varrho_{n-k} \nabla_+ g_{j-n}(t - t_k^*)$$

for any k , all j , and every t with $t_k^* + d_*/\varepsilon \leq t$. Young's inequality for convolutions implies via $\|\varrho * \cdot\|_2 \leq \|\varrho\|_1 \|\cdot\|_2$ the estimate

$$\left(\sum_{j \in \mathbb{Z}} |\nabla_{+r_{\text{reg},j}^{(k)}}(t)|^2 \right)^{1/2} \leq \frac{C}{(1+t-t_k^*)^{3/4}},$$

and as in the proof of Lemma 3.10 – see (3.30) and Figure 3.6 – we deduce

$$\sum_{k=1}^{K_\varepsilon} \left(\sum_{j \in \mathbb{Z}} |\nabla_{+r_{\text{reg},j}^{(k)}}(t)|^2 \right)^{1/2} \leq C \sum_{l=1}^{\lfloor \varepsilon t / (2d_*) \rfloor} \left(\frac{\varepsilon}{d_* l} \right)^{3/4} \leq C \varepsilon^{1/2}.$$

The assertion is now a direct consequence of the triangle inequality. \square

4 Justification of the hysteretic free boundary problem

In order to pass to the macroscopic limit, we choose a scaling parameter $0 < \varepsilon \ll 1$ and regard the lattice data as continuous functions in the macroscopic time τ that are piecewise constant with respect to the macroscopic space variable as they depend only on the integer part of ξ/ε . More precisely, in accordance with (1.6) we write

$$\xi = \varepsilon(j_\xi + \zeta_\xi) \quad \text{with} \quad j_\xi \in \mathbb{Z}, \quad \zeta_\xi \in (-1/2, +1/2], \quad (4.1)$$

and define

$$P_\varepsilon(\tau, \xi) := p_{j_\xi}(\tau/\varepsilon^2), \quad R_{\text{reg},\varepsilon}(\tau, \xi) := \sum_{k \geq 1} r_{\text{reg},j_\xi}^{(k)}(\tau/\varepsilon^2).$$

Furthermore, by similar formulas we construct functions U_ε , $R_{\text{res},\varepsilon}$, and $R_{\text{neg},\varepsilon}$ from their microscopic counterparts, and setting

$$Q_\varepsilon(\tau, \xi) := \sum_{n \in \mathbb{N}} g_{j_\xi - n}(\tau/\varepsilon^2) p_n(0)$$

we infer from (3.9) the identity

$$P_\varepsilon = Q_\varepsilon - (R_{\text{reg},\varepsilon} + R_{\text{neg},\varepsilon} + R_{\text{res},\varepsilon}). \quad (4.2)$$

Finally, we introduce two discrete analogs to the macroscopic interface curve via

$$\Xi_\varepsilon^*(\tau) := \varepsilon \sum_{k \geq 1} k \chi_{[t_{k-1}^*, t_k^*)}(\tau/\varepsilon^2), \quad \Xi_\varepsilon^\#(\tau) := \varepsilon \sum_{k \geq 1} k \chi_{[t_{k-1}^\#, t_k^\#)}(\tau/\varepsilon^2)$$

and approximate the macroscopic phase field by

$$M_\varepsilon(\tau, \xi) := \begin{cases} -1 & \text{if } \xi > \Xi_\varepsilon^\#(\tau), \\ +1 & \text{if } \xi < \Xi_\varepsilon^*(\tau), \\ 0 & \text{otherwise;} \end{cases} \quad (4.3)$$

see Figure 4.1 for an illustration.

4.1 Compactness results

Our first result concerns the compactness of the scaled lattice data and extends the arguments for the bilinear case $\kappa = \infty$ from [HH13].

Proposition 4.1 (Compactness). *Under Assumption 3.1 there exist (not relabeled) sequences such that the following statements are satisfied for $\varepsilon \rightarrow 0$:*

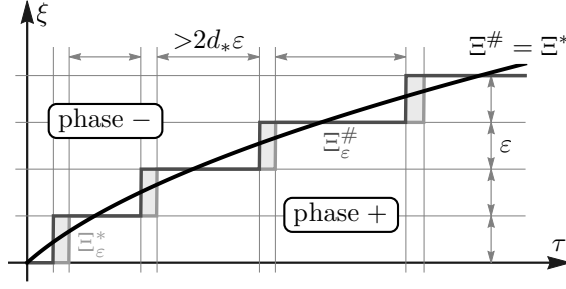


Figure 4.1: Cartoon of the macroscopic phase interface, both on the discrete level (piecewise constant graphs $\Xi_\varepsilon^\#$ and Ξ_ε^* in dark and light gray, respectively) and in the continuum limit (black curve Ξ). All spinodal passages and excursions take place inside the shaded region, whose macroscopic area is bounded from above by $\varepsilon\tau_{\text{fin}}$ and typically of order $\varepsilon^2 |\ln \varepsilon|$.

1. (convergence of interfaces) *We have*

$$|\Gamma_\varepsilon| \rightarrow 0 \quad \text{where} \quad \Gamma_\varepsilon := \{(\tau, \xi) : \Xi_\varepsilon^*(\tau) \leq \xi \leq \Xi_\varepsilon^\#(\tau), 0 \leq \tau \leq \tau_{\text{fin}}\}, \quad (4.4)$$

and both $\Xi_\varepsilon^\#$ and Ξ_ε^* converge strongly in $L^\infty([0, \tau_{\text{fin}}])$ to the same Lipschitz function Ξ .

2. (strong convergence of fields) *There exist bounded functions U , P , and M such that*

$$U_\varepsilon \rightarrow U, \quad P_\varepsilon \rightarrow P, \quad M_\varepsilon \rightarrow M \quad \text{strongly in} \quad L_{\text{loc}}^s([0, \tau_{\text{fin}}] \times \mathbb{R}) \quad (4.5)$$

for any $1 \leq s < \infty$. Moreover, P is locally Hölder-continuous in space and time on $[0, \tau_{\text{fin}}] \times \mathbb{R}$ and we have $P_\varepsilon(\tau, \cdot) \rightarrow P(\tau, \cdot)$ strongly in $L_{\text{loc}}^s(\mathbb{R})$ for any $\tau \in [0, \tau_{\text{fin}}]$.

3. (weak convergence of spatial derivatives) *P admits the weak derivative $\partial_\xi P$ for any $\tau \in [0, \tau_{\text{fin}}]$ and we have*

$$\nabla_{+\varepsilon} P_\varepsilon \rightarrow \partial_\xi P \quad \text{weakly in} \quad L_{\text{loc}}^2([0, \tau_{\text{fin}}] \times \mathbb{R}), \quad (4.6)$$

where $\nabla_{+\varepsilon}$ denotes the right-sided difference approximation of ∂_ξ on $\varepsilon\mathbb{Z}$.

Here, $0 < \tau_{\text{fin}} < \infty$ denotes a fixed macroscopic time that is independent of ε .

Proof. Interface curve: The Lebesgue measure of Γ_ε can be estimated by

$$|\Gamma_\varepsilon| \leq \varepsilon\tau_{\text{fin}} \quad (4.7)$$

because Proposition 2.2 ensures that for each time τ there is at most one particle inside the spinodal region. Moreover, the jumps of both Ξ_ε^* and $\Xi_\varepsilon^\#$ are always of size ε and the time between two jumps is bounded from below by $2d_*\varepsilon$ due to Corollary 3.2; see Figure 4.1 for an illustration. By approximation with piecewise linear functions we thus deduce the strong compactness of both Ξ_ε^* and $\Xi_\varepsilon^\#$ as well as the Lipschitz continuity of any accumulation point, see [HH13, Lemma 3.9] for the details. Finally, (4.7) implies that the accumulations points of $\Xi_\varepsilon^\#$ and Ξ_ε^* coincide.

Negligible and residual fluctuations: For given τ , Corollary 3.8 and Lemma 3.9 yield

$$\|R_{\text{neg},\varepsilon}(\tau, \cdot)\|_{L^1(\mathbb{R})} \leq C\sqrt{\varepsilon} \quad \text{and} \quad \|R_{\text{res},\varepsilon}(\cdot, \tau)\|_{L^1(\mathbb{R})} \leq C\varepsilon,$$

and Corollary 3.11 provides

$$\|R_{\text{neg},\varepsilon}(\tau, \cdot)\|_{L^\infty(\mathbb{R})} + \|R_{\text{res},\varepsilon}(\tau, \cdot)\|_{L^\infty(\mathbb{R})} \leq C.$$

By Hölder's inequality and interpolation we thus find

$$R_{\text{neg},\varepsilon}(\tau, \cdot) \rightarrow 0 \quad \text{and} \quad R_{\text{res},\varepsilon}(\tau, \cdot) \rightarrow 0 \quad \text{strongly in} \quad L^s(\mathbb{R}), \quad (4.8)$$

as well as a corresponding convergence result in $L^s([0, \tau_{\text{fin}}] \times \mathbb{R})$.

Essential fluctuations: From Lemma 3.10 we infer the estimate

$$|R_{\text{reg},\varepsilon}(\tau_2, \xi_2) - R_{\text{reg},\varepsilon}(\tau_1, \xi_1)| \leq C \left(|\tau_2 - \tau_1|^{1/4} + |\xi_2 - \xi_1|^{1/2} \right) + C\varepsilon^{1/2}$$

and conclude that the piecewise constant function $R_{\text{reg},\varepsilon}$ is almost Hölder continuous with small spatial jumps of order $\varepsilon^{1/2}$. A variant of the Arzelà-Ascoli theorem – see [HH13, Lemma 3.10] – provides a Hölder continuous function R along with a subsequence of $\varepsilon \rightarrow 0$ such that

$$R_{\text{reg},\varepsilon} \rightarrow R \quad \text{strongly in } L^\infty([0, \tau_{\text{fin}}] \times \mathbb{R})$$

as well as

$$R_{\text{reg},\varepsilon}(\tau, \cdot) \rightarrow R(\tau, \cdot) \quad \text{strongly in } L^\infty(\mathbb{R}) \quad (4.9)$$

for any given τ .

Other fields: The compactness of Q_ε , which represent the scaled solutions of the discrete heat equation with macroscopic initial data as in Assumption 3.1, as well as the regularity of any accumulation point can be proven in many ways; see for instance [HH13, Lemma 3.11] for an approach via Hölder regularity. Extracting another subsequence we can therefore assume that

$$Q_\varepsilon(\tau, \cdot) \rightarrow Q(\tau, \cdot) \quad \text{strongly in } L^s_{\text{loc}}(\mathbb{R}) \quad (4.10)$$

and

$$Q_\varepsilon \rightarrow Q \quad \text{strongly in } L^s_{\text{loc}}([0, \tau_{\text{fin}}] \times \mathbb{R})$$

hold for some continuous function Q , and together with (4.2), (4.8), and (4.9) we obtain the claimed convergence properties of P_ε . Moreover, (4.3) and (4.4) imply the convergence of M_ε .

Spatial gradient: For fixed τ , Lemma 3.12 ensures that

$$\|\nabla_{+\varepsilon} R_{\text{reg},\varepsilon}(\tau, \cdot)\|_{L^2(\mathbb{R})} \leq C,$$

while Assumption 3.1 combined with the properties of the discrete heat kernel guarantees

$$\|\nabla_{+\varepsilon} Q_\varepsilon(\tau, \cdot)\|_{L^2_{\text{loc}}(\mathbb{R})} \leq \alpha.$$

In particular, $\nabla_{+\varepsilon}(R_{\text{reg},\varepsilon}(\tau, \cdot) + Q_\varepsilon(\tau, \cdot))$ is weakly compact in $L^2_{\text{loc}}(\mathbb{R})$ and any accumulation point $Z(\tau, \cdot)$ satisfies

$$\int_{\mathbb{R}} Z(\tau, \xi) \Psi(\xi) d\xi = - \lim_{\varepsilon \rightarrow 0} \int_{\mathbb{R}} (R_{\text{reg},\varepsilon}(\tau, \xi) + Q_\varepsilon(\tau, \xi)) \nabla_{-\varepsilon} \Psi(\xi) d\xi = - \int_{\mathbb{R}} P(\tau, \xi) \partial_\xi \Psi(\xi) d\xi$$

thanks to (4.8)–(4.10), where $\Psi \in C_c^\infty(\mathbb{R})$ is an arbitrary smooth test function and $\nabla_{-\varepsilon}$ abbreviates the left-sided difference operator on $\varepsilon\mathbb{Z}$. This implies the existence of the weak derivative $\partial_\xi P(\tau, \cdot) \in L^2_{\text{loc}}(\mathbb{R})$ for any τ . Towards (4.6) we fix $\lambda > 0$, define a nonnegative and piecewise constant function $\Psi_\varepsilon \in L^\infty(\mathbb{R})$ in consistency with (4.1) by

$$\Psi_\varepsilon(\xi) := \exp(-\lambda \varepsilon |j_\xi|),$$

and verify by direct computations that

$$|\nabla_{+\varepsilon} \Psi_\varepsilon(\xi)| \leq C\lambda \left(\Psi_\varepsilon(\xi) + \chi_{[-\varepsilon/2, +\varepsilon/2]}(\xi) \right).$$

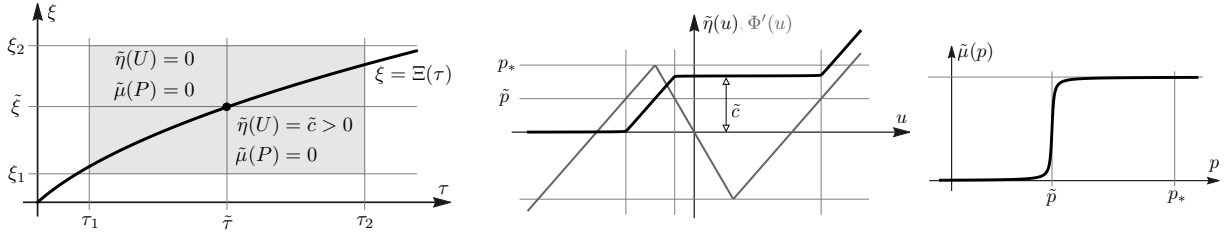


Figure 4.2: *Left panel.* Illustration of the entropy argument in the proof of Theorem 4.2, which reveals that $P(\tilde{\tau}, \tilde{\xi}) < p_*$ implies $\frac{d}{d\tau}\Xi(\tilde{\tau}) = 0$. *Center and right panel.* Smooth approximations of the entropy pair $(\tilde{\eta}, \tilde{\mu})$ from (4.19).

Evaluating Proposition 2.6 with $\psi_j = \Psi(\varepsilon j)$ and inserting the scaling (1.6) we then find

$$\begin{aligned}
\int_0^{\tau_{\text{fin}}} \int_{\mathbb{R}} \Psi_\varepsilon (\nabla_{+\varepsilon} P_\varepsilon)^2 d\xi d\tau &\leq \int_{\mathbb{R}} \Psi_\varepsilon \Phi(U_\varepsilon) d\xi - \int_0^{\tau_{\text{fin}}} \int_{\mathbb{R}} P_\varepsilon (\nabla_{+\varepsilon} \Psi_\varepsilon) (\nabla_{+\varepsilon} P_\varepsilon) d\xi d\tau \\
&\leq C + C \int_0^{\tau_{\text{fin}}} \int_{\mathbb{R}} \Psi_\varepsilon |\nabla_{+\varepsilon} P_\varepsilon| d\xi d\tau \\
&\leq C + C \int_0^{\tau_{\text{fin}}} \int_{\mathbb{R}} \Psi_\varepsilon d\xi d\tau + \frac{1}{2} \int_0^{\tau_{\text{fin}}} \int_{\mathbb{R}} \Psi_\varepsilon (\nabla_{+\varepsilon} P_\varepsilon)^2 d\xi d\tau.
\end{aligned}$$

Here, C depends on λ but not on ε and we omitted the arguments of the functions to ease the notation. Since λ is arbitrary we conclude that $\nabla_{+\varepsilon} P_\varepsilon$ is weakly compact in $L^2_{\text{loc}}([0, \tau_{\text{fin}}] \times \mathbb{R})$. Moreover, any accumulation Z point fulfills

$$\int_0^{\tau_{\text{fin}}} \int_{\mathbb{R}} Z \Psi d\xi d\tau = - \lim_{\varepsilon \rightarrow 0} \int_0^{\tau_{\text{fin}}} \int_{\mathbb{R}} P_\varepsilon \nabla_{-\varepsilon} \Psi d\xi d\tau = \int_0^{\tau_{\text{fin}}} \int_{\mathbb{R}} \partial_\xi P \Psi d\xi d\tau$$

for any test function $\Psi \in C_c^\infty((0, \tau_{\text{fin}}) \times \mathbb{R})$, so (4.6) follows from the standard argument that compactness and uniqueness of accumulation points imply convergence, which holds also with respect to the weak topology in L^2_{loc} . \square

4.2 Passage to the macroscopic limit

Next we derive the hysteretic free boundary problem from Main Result 1.4 along converging sequences and justify the hysteretic flow rule. In the bilinear case $\kappa = \infty$, there exists a straightforward argument based on the Hölder continuity of P and the precise information on the microscopic phase transitions; see [HH13, proof of Theorem 3.6]. In the trilinear case, however, we have to argue in a more sophisticated way due to the lack of vanishing ℓ^∞ -bounds for the negligible fluctuations. In what follows we therefore employ the notion of entropy solutions that has been introduced in [Plo94, EP04] in the context of the viscous regularization (1.3).

Theorem 4.2 (Limit dynamics along sequences). *Any limit from Proposition 4.1 has the following properties, where $\Omega := [0, \tau_{\text{fin}}] \times \mathbb{R}$ and $\Gamma := \{(\tau, \xi) \in \Omega : \xi = \Xi(\tau)\}$:*

1. (free boundary problem with Stefan condition) (P, Ξ) is a distributional solution of

$$\partial_\tau P = \partial_\xi^2 P \quad \text{in } \Omega \setminus \Gamma, \quad \llbracket P \rrbracket = 0 \quad \text{and} \quad 2 \frac{d}{d\tau} \Xi = \llbracket \partial_\xi P \rrbracket \quad \text{on } \Gamma \quad (4.11)$$

and attains the initial data $(P(0), 0)$. Moreover, we have

$$M(\tau, \xi) = \text{sgn}(U(\tau, \xi)) = \text{sgn}(\Xi(\tau) - \xi) \quad \text{for } \xi \neq \Xi(\tau) \quad (4.12)$$

as well as

$$P(\tau, \xi) \geq -p_* \quad \text{for } \xi \leq \Xi(\tau), \quad P(\tau, \xi) \in [-p_*, +p_*] \quad \text{for } \xi \geq \Xi(\tau) \quad (4.13)$$

and $\frac{d}{d\tau}\Xi(\tau) \geq 0$ for almost all τ .

2. (hysteretic flow rule and entropy balances) *The implication*

$$P(\tau, \Xi(\tau)) < p_* \implies \frac{d}{d\tau}\Xi(\tau) = 0 \quad (4.14)$$

holds for almost all τ and the entropy inequality

$$\partial_\tau \eta(U) - \partial_\xi (\mu(P) \partial_\xi P) \leq 0 \quad (4.15)$$

is satisfied in the sense of distributions for any smooth entropy pair (η, μ) as in (1.12).

Proof. Stefan problem: By construction we have

$$M_\varepsilon(\tau, \xi) = U_\varepsilon(\tau, \xi) - P_\varepsilon(\tau, \xi) = \text{sgn } U_\varepsilon(\tau, \xi) \quad \text{for } (\tau, \xi) \notin \Gamma_\varepsilon$$

with Γ_ε as in (4.4), and taking the limit $\varepsilon \rightarrow 0$ we obtain (4.12) by (4.5) and the pointwise convergence of both Ξ_ε^* and $\Xi_\varepsilon^\#$ to Ξ . Moreover, the lattice ODE (1.4) combined with the scaling (1.6) gives rise to

$$\int_0^{\tau_{\text{fin}}} \int_{\mathbb{R}} U_\varepsilon \partial_\tau \Psi \, d\xi \, d\tau = - \int_0^{\tau_{\text{fin}}} \int_{\mathbb{R}} P_\varepsilon \Delta_\varepsilon \Psi \, d\xi \, d\tau,$$

for any test function $\Psi \in C_c^\infty((0, \tau_{\text{fin}}) \times \mathbb{R})$, where $\Delta_\varepsilon = \nabla_{-\varepsilon} \nabla_{+\varepsilon}$ is the finite difference approximation of ∂_ξ^2 on $\varepsilon\mathbb{Z}$. Using (4.4) and (4.5) we pass again to the limit $\varepsilon \rightarrow 0$ and find

$$\int_0^{\tau_{\text{fin}}} \int_{\mathbb{R}} (P + M) \partial_\tau \Psi \, d\xi \, d\tau = - \int_0^{\tau_{\text{fin}}} \int_{\mathbb{R}} P \partial_\xi^2 \Psi \, d\xi \, d\tau = \int_0^{\tau_{\text{fin}}} \int_{\mathbb{R}} \partial_\xi P \partial_\xi \Psi \, d\xi \, d\tau.$$

This is the weak formulation of (4.11) since the properties of Φ from (1.13) along with (4.5) and the continuity of P ensure that

$$\llbracket U(\tau) \rrbracket = U(\tau, \Xi(\tau) + 0) - U(\tau, \Xi(\tau) - 0) = -2u_*$$

holds for almost all τ and ξ . Moreover, (4.13) and the monotonicity of Ξ also follow from their discrete counterparts, see Definition 2.1 and Propositions 2.2 and 4.1.

Entropy inequalities: Let $0 \leq \tau_1 < \tau_2 \leq \tau_{\text{fin}}$ be given and $\Psi \in C_c^\infty([0, \tau_{\text{fin}}] \times \mathbb{R})$ be a nonnegative test function. Proposition 2.6 gives rise to the entropy inequality

$$\int_{\mathbb{R}} \eta(U_\varepsilon) \Psi_\varepsilon \, d\xi \Big|_{\tau=\tau_1}^{\tau=\tau_2} \leq \int_{\tau_1}^{\tau_2} \int_{\mathbb{R}} \left(\eta(U_\varepsilon) \partial_\tau \Psi_\varepsilon - \mu(P_\varepsilon) (\nabla_{+\varepsilon} \Psi_\varepsilon) (\nabla_{+\varepsilon} P_\varepsilon) \right) d\xi \, d\tau$$

where Ψ_ε denotes the ε -approximation of Ψ , which is piecewise constant in space and defined by

$$\Psi_\varepsilon(\tau, \varepsilon j + \zeta) = \Psi(\tau, \varepsilon j) \quad \text{for all } j \in \mathbb{Z}, \tau \in [0, \tau_{\text{fin}}], \zeta \in [-\varepsilon/2, \varepsilon/2).$$

Thanks to the smoothness of Ψ , the compactness of $\text{supp } \Psi$, the weak convergence of $\nabla_{+\varepsilon} P_\varepsilon$, and the strong convergence of P_ε – see (4.5) and (4.6) – we can pass to the limit $\varepsilon \rightarrow 0$ and obtain

$$\int_{\mathbb{R}} \eta(U) \Psi \, d\xi \Big|_{\tau=\tau_1}^{\tau=\tau_2} \leq \int_{\tau_1}^{\tau_2} \int_{\mathbb{R}} \left(\eta(U) \partial_\tau \Psi - \mu(P) \partial_\xi \Psi \partial_\xi P \right) d\xi \, d\tau, \quad (4.16)$$

which in turn yields (4.15) in the sense of distributions if we choose $\tau_1 = 0$, $\tau_2 = \tau_{\text{fin}}$ and a test function Ψ that vanishes for $\tau = 0$ and $\tau = \tau_{\text{fin}}$.

Justification of the flow rule: Let $\tilde{\tau} \in [0, \tau_{\text{fin}}]$ be fixed with

$$-p_* \leq P(\tilde{\tau}, \tilde{\xi}) < +p_*, \quad \tilde{\xi} := \Xi(\tilde{\tau}). \quad (4.17)$$

Thanks to the continuity of both Ξ and P we can choose positions $\xi_1 < \xi_2$ and times $\tau_1 < \tau_2$ along with a number \tilde{p} such that

$$\xi_1 \leq \tilde{\xi} \leq \xi_2, \quad \tau_1 \leq \tilde{\tau} \leq \tau_2, \quad \xi_1 < \Xi(\tau) < \xi_2 \quad \text{for all } \tau \in [\tau_1, \tau_2]$$

and

$$-p_* \leq P(\tau, \xi) < \tilde{p} < p_* \quad \text{for all } (\tau, \xi) \in [\tau_1, \tau_2] \times [\xi_1, \xi_2].$$

This construction is illustrated in the left panel in Figure 4.2. Moreover, considering nonnegative test functions $\Psi \in C_c((\xi_1, \xi_2))$ in (4.16) we obtain

$$\int_{\xi_1}^{\xi_2} \eta(U(\tau_2, \xi)) \Psi(\xi) d\xi - \int_{\xi_1}^{\xi_2} \eta(U(\tau_1, \xi)) \Psi(\xi) d\xi \leq - \int_{\tau_1}^{\tau_2} \int_{\xi_1}^{\xi_2} \mu(P(\tau, \xi)) \partial_\xi \Psi(\xi) \partial_\xi P(\tau, \xi) d\xi d\tau, \quad (4.18)$$

and by approximation with smooth densities and fluxes we deduce that (4.18) holds also for the non-smooth entropy pair

$$\tilde{\mu}(p) := \begin{cases} 0 & \text{for } p \leq \tilde{p}, \\ +1 & \text{for } p > \tilde{p}, \end{cases} \quad \tilde{\eta}(u) = \int_{-\infty}^u \tilde{\mu}(\Phi'(\bar{u})) d\bar{u}. \quad (4.19)$$

Direct computations reveal that (4.18) reduces to

$$\tilde{c} \int_{\xi_1}^{\Xi(\tau_2)} \Psi(\xi) d\xi - \tilde{c} \int_{\xi_1}^{\Xi(\tau_1)} \Psi(\xi) d\xi \leq 0$$

for some constant $\tilde{c} > 0$, and since Ψ was arbitrary we get

$$\Xi(\tau_2) \leq \Xi(\tau_1).$$

On the other hand, Ξ is also non-decreasing by construction. We thus arrive at

$$\Xi(\tau) = \Xi(\tilde{\tau}) \quad \text{for all } \tau \in [\tau_1, \tau_2]$$

and conclude that (4.17) implies $\frac{d}{d\tau} \Xi(\tau) = 0$ for almost all $\tau \in [\tau_1, \tau_2]$. In particular, the interface satisfies (4.14). \square

The final ingredient to the proof of the main result from §1 is to extend the convergence along sequences to convergence of the whole family $\varepsilon \rightarrow 0$. This follows from the fact that for given macroscopic initial data there exists precisely one solution to the limit model from §1. Since the arguments are the same for the bilinear and the trilinear case, we refer to [HH13, Theorem 3.18] for the proof and to [Hil89, Vis06] for the key estimates. A similar uniqueness result can be found in [MTT09].

Conflict of Interest

The authors declare that they have no conflict of interest.

References

- [BBDPU93] G. I. Barenblatt, M. Bertsch, R. Dal Passo, and M. Ughi. A degenerate pseudoparabolic regularization of a nonlinear forward-backward heat equation arising in the theory of heat and mass exchange in stably stratified turbulent shear flow. *SIAM J. Math. Anal.*, 24(6):1414–1439, 1993.
- [BBMN12] G. Bellettini, L. Bertini, M. Mariani, and M. Novaga. Convergence of the One-Dimensional Cahn–Hilliard Equation. *SIAM J. Math. Anal.*, 44(5):3458–3480, 2012.
- [BCT17] E. Bonetti, P. Colli, and G. Tomassetti. A non-smooth regularization of a forward-backward parabolic equation. *Math. Models Methods Appl. Sci.*, 27(4):641–661, 2017.
- [BGN13] G. Bellettini, C. Geldhauser, and M. Novaga. Convergence of a semidiscrete scheme for a forward-backward parabolic equation. *Adv. Differential Equations*, 18(5/6):495–522, 2013.
- [Bra14] A. Braides. *Local minimization, variational evolution and Γ -convergence*, volume 2094 of *Lecture Notes in Mathematics*. Springer, Cham, 2014.
- [BST16] M. Bertsch, F. Smarrazzo, and A. Tesei. Nonuniqueness of solutions for a class of forward-backward parabolic equations. *Nonlinear Anal.*, 137:190–212, 2016.
- [EG09] S. Esedoğlu and J. B. Greer. Upper bounds on the coarsening rate of discrete, ill-posed nonlinear diffusion equations. *Comm. Pure Appl. Math.*, 62(1):57–81, 2009.
- [Ell85] C. M. Elliott. The Stefan problem with a nonmonotone constitutive relation. *IMA J. Appl. Math.*, 35(2):257–264, 1985. Special issue: IMA conference on crystal growth (Oxford, 1985).
- [EP04] L. C. Evans and M. Portilheiro. Irreversibility and hysteresis for a forward-backward diffusion equation. *Math. Models Methods Appl. Sci.*, 14(11):1599–1620, 2004.
- [ES08] S. Esedoğlu and D. Slepčev. Refined upper bounds on the coarsening rate of discrete, ill-posed diffusion equations. *Nonlinearity*, 21(12):2759–2776, 2008.
- [GN11] C. Geldhauser and M. Novaga. A semidiscrete scheme for a one-dimensional Cahn–Hilliard equation. *Interfaces Free Bound.*, 13(3):327–339, 2011.
- [GST13] P. Gurevich, R. Shamin, and S. Tikhomirov. Reaction-diffusion equations with spatially distributed hysteresis. *SIAM J. Math. Anal.*, 45(3):1328–1355, 2013.
- [GT10] B. H. Gilding and A. Tesei. The Riemann problem for a forward-backward parabolic equation. *Phys. D*, 239(6):291–311, 2010.
- [GT16] P. Gurevich and S. Tikhomirov. Rattling in spatially discrete diffusion equations with hysteresis. arXiv preprint no. 1601.05728, 2016.
- [HH13] M. Helmers and M. Herrmann. Interface dynamics in discrete forward-backward diffusion equations. *Multiscale Model. Simul.*, 11(4):1261–1297, 2013.
- [Hil89] M. Hilpert. On uniqueness for evolution problems with hysteresis. In *Mathematical models for phase change problems (Óbidos, 1988)*, volume 88 of *Internat. Ser. Numer. Math.*, pages 377–388. Birkhäuser, Basel, 1989.
- [Höl83] K. Höllig. Existence of infinitely many solutions for a forward backward heat equation. *Trans. Amer. Math. Soc.*, 278(1):299–316, 1983.

- [Hol16] M. Holle. Microstructure in forward-backward lattice diffusion. Master's thesis, University of Bonn, 2016.
- [HPO04] D. Horstmann, K. J. Painter, and H. G. Othmer. Aggregation under local reinforcement: from lattice to continuum. *European J. Appl. Math.*, 15(5):546–576, 2004.
- [LM12] P. Lafitte and C. Mascia. Numerical exploration of a forward-backward diffusion equation. *Math. Models Methods Appl. Sci.*, 22(6):1250004, 33, 2012.
- [MT12] A. Mielke and L. Truskinovsky. From discrete visco-elasticity to continuum rate-independent plasticity: rigorous results. *Arch. Ration. Mech. Anal.*, 203(2):577–619, 2012.
- [MTT09] C. Mascia, A. Terracina, and A. Tesei. Two-phase entropy solutions of a forward-backward parabolic equation. *Arch. Ration. Mech. Anal.*, 194(3):887–925, 2009.
- [NCP91] A. Novick-Cohen and R. L. Pego. Stable patterns in a viscous diffusion equation. *Trans. Amer. Math. Soc.*, 324(1):331–351, 1991.
- [OR07] F. Otto and M.G. Reznikoff. Slow motion of gradient flows. *J. Differential Equations*, 237(2):372–420, 2007.
- [Pad04] V. Padrón. Effect of aggregation on population recovery modeled by a forward-backward pseudoparabolic equation. *Trans. Amer. Math. Soc.*, 356(7):2739–2756 (electronic), 2004.
- [Pie10] M. Pierre. Uniform convergence for a finite-element discretization of a viscous diffusion equation. *IMA J. Numer. Anal.*, 30(2):487–511, 2010.
- [Plo94] P. I. Plotnikov. Passing to the limit with respect to viscosity in an equation with variable parabolicity direction. *Differential Eqns.*, 30(4):614–622, 1994.
- [PM90] P. Perona and J. Malik. Scale-space and edge-detection using anisotropic diffusion. *IEEE Trans. Pattern Anal. Machine Intell.*, 12(7):629–639, 1990.
- [PSV12] M. A. Peletier, G. Savaré, and M. Veneroni. Chemical reactions as Γ -limit of diffusion [revised reprint of mr2679596]. *SIAM Rev.*, 54(2):327–352, 2012.
- [Ser11] S. Serfaty. Gamma-convergence of gradient flows on Hilbert and metric spaces and applications. *Discrete Contin. Dyn. Syst.*, 31(4):1427–1451, 2011.
- [ST10] F. Smarrazzo and A. Tesei. Long-time behavior of solutions to a class of forward-backward parabolic equations. *SIAM J. Math. Anal.*, 42(3):1046–1093, 2010.
- [ST11] F. Smarrazzo and A. Tesei. Some recent results concerning a class of forward-backward parabolic equations. *Atti Accad. Naz. Lincei Cl. Sci. Fis. Mat. Natur. Rend. Lincei (9) Mat. Appl.*, 22(2):175–188, 2011.
- [Ter14] A. Terracina. Non-uniqueness results for entropy two-phase solutions of forward-backward parabolic problems with unstable phase. *J. Math. Anal. Appl.*, 413(2):963–975, 2014.
- [Ter15] A. Terracina. Two-phase entropy solutions of forward-backward parabolic problems with unstable phase. *Interfaces Free Bound.*, 17(3):289–315, 2015.
- [Vis06] A. Visintin. Quasilinear parabolic P.D.E.s with discontinuous hysteresis. *Ann. Mat. Pura Appl.*, 185(4):487–519, 2006.
- [YW03] J. Yin and Ch. Wang. Young measure solutions of a class of forward-backward diffusion equations. *J. Math. Anal. Appl.*, 279(2):659–683, 2003.

- [Zha06] K. Zhang. On existence of weak solutions for one-dimensional forward-backward diffusion equations. *J. Differential Equations*, 220(2):322–353, 2006.